GJI Geomagnetism, rock magnetism and palaeomagnetism

On flow magnitude and field-flow alignment at Earth's core surface

Christopher C. Finlay[1] and Hagay Amit[2]

[1]*Institut für Geophysik, Sonneggstrasse 5, ETH Zürich, Zürich,* CH-8092, *Switzerland. E-mail: cfinlay@erdw.ethz.ch*
[2]*CNRS UMR 6112, Université de Nantes, Laboratoire de Planétologie et de Géodynamique,* 2 *Rue de la Houssinière, Nantes,* F-44000, *France*

SUMMARY

We present a method to estimate the typical magnitude of flow close to Earth's core surface based on observational knowledge of the geomagnetic main field (MF) and its secular variation (SV), together with prior information concerning field-flow alignment gleaned from numerical dynamo models. An expression linking the core surface flow magnitude to spherical harmonic spectra of the MF and SV is derived from the magnetic induction equation. This involves the angle γ between the flow and the horizontal gradient of the radial field. We study γ in a suite of numerical dynamo models and discuss the physical mechanisms that control it. Horizontal flow is observed to approximately follow contours of the radial field close to high-latitude flux bundles, while more efficient induction occurs at lower latitudes where predominantly zonal flows are often perpendicular to contours of the radial field. We show that the amount of field-flow alignment depends primarily on a magnetic modified Rayleigh number $\mathrm{Ra}_\eta = \alpha g_0 \Delta T D / \eta \Omega$, which measures the vigour of convective driving relative to the strength of magnetic dissipation. Synthetic tests of the flow magnitude estimation scheme are encouraging, with results differing from true values by less than 8 per cent. Application to a high-quality geomagnetic field model based on satellite observations (the *xCHAOS* model in epoch 2004.0) leads to a flow magnitude estimate of 11–14 km yr^{-1}, in accordance with previous estimates. When applied to the historical geomagnetic field model *gufm1* for the interval 1840.0–1990.0, the method predicts temporal variations in flow magnitude similar to those found in earlier studies. The calculations rely primarily on knowledge of the MF and SV spectra; by extrapolating these beyond observed scales the influence of small scales on flow magnitude estimates is assessed. Exploring three possible spectral extrapolations we find that the magnitude of the core surface flow, including small scales, is likely less than 50 km yr^{-1}.

Key words: Dynamo: theories and simulations; Satellite magnetics; Planetary interiors.

1 INTRODUCTION

Flow of electrically conducting fluid in the Earth's liquid outer core generates the geomagnetic field via motional induction. Detailed understanding of this process requires reliable, observation-based, estimates of the typical magnitude of the core flow $\mathcal{U}$. For example, knowledge of $\mathcal{U}$ is needed to calculate fundamental non-dimensional parameters such as the magnetic Reynolds number $\mathrm{Rm} = \mathcal{U}\mathcal{L}/\eta$ and the Rossby number $\mathrm{Ro} = \mathcal{U}/\Omega\mathcal{L}$, where $\mathcal{L}$ is a characteristic length scale, η is the magnetic diffusivity and Ω is the angular rotation rate of the system. Rm and Ro, respectively, diagnose the kinematic and dynamic regime of dynamos driven by rotating convection. Without robust knowledge of $\mathcal{U}$ it is difficult to assess how close numerical dynamo models are to an earth-like regime. Since present simulations yield results spanning a wide range of Rm (Roberts & Glatzmaier 2000; Christensen & Tilgner 2004) and Ro (Christensen & Aubert 2006; Olson & Christensen 2006; Sreenivasan & Jones 2006) that encompass distinct be-

haviours ranging from non-reversing and dipole-dominated, to reversing multipolar fields (Kutzner & Christensen 2002), it would be extremely helpful if geomagnetic observations could place tighter limits on acceptable values of Ro and Rm. In this study, we attempt to make some progress towards this goal by developing a new technique to estimate the typical magnitude of horizontal flow at the Earth's core surface $\langle u_H \rangle$ which hereafter is used as a proxy for $\mathcal{U}$.

Previous efforts to estimate $\langle u_H \rangle$ have focused on inferences from observed changes [i.e. secular variation (SV)] in the Earth's core-generated main field (MF), following an idea originating with Elsasser (1939). From scale analysis of the magnetic induction equation (and neglecting magnetic diffusion), one can estimate the order of magnitude of flow required to explain the observed SV, given the observed magnitude of the MF and an assumed length scale for core motions (Elsasser 1946; Elsasser 1950a). A later idea was to determine the angular speed of foci of non-dipole field at the Earth's surface, and then to calculate the magnitude of flow at the core surface necessary to produce this motion (Bullard *et al.* 1950).

Roberts & Scott (1965) pointed out that detailed maps of the horizontal flow $\boldsymbol{u}_H$, just below the thin Ekman–Hartmann boundary layer at the top of the core, could be obtained from spherical harmonic models of the radial MF, B_r and its SV, $\partial B_r/\partial t$, again provided magnetic diffusion can be neglected; Vestine and co-workers proceeded to calculate such maps (see Kahle *et al.* 1967a; Kahle *et al.* 1967b). Later Backus (1968) pointed out that such core flow determinations are inherently non-unique, due to a lack of information from the radial frozen-flux induction equation concerning the solenoidal part of the product $B_r \, \boldsymbol{u}_H$. A simple example of this difficulty is that flow along null flux contours (where $B_r = 0$) produces no SV, so it is unconstrained by observations of the MF evolution. Backus (1968) also proved that unique estimates of certain flow components were possible at specific topological locations. These point estimates provide useful direct estimates (see, e.g. Booker 1969; Whaler & Holme 2007), but unfortunately sample only a very small portion of the core surface, capture only one component of the flow, and are subject to difficulties in estimating the amplitude of errors on point estimates of the MF at the core surface.

Over the past three decades, modern core flow inversion studies have exploited a variety of dynamical constraints and truncation and regularization assumptions (for comprehensive reviews see Bloxham & Jackson 1991; Holme 2007; Finlay et al. 2010) in an attempt to mitigate the effects of non-uniqueness. In such studies, estimates of $\langle \boldsymbol{u}_H \rangle$ are derived from the root mean square (rms) magnitude of $\boldsymbol{u}_H$ at the core surface. In Table 1 we present a selection of published flow magnitude estimates. These encompass both early foci tracking and point estimate methods, and results from more recent flow inversions involving a diverse range of dynamical assumptions, inversion strategies and sets of magnetic observations. These previous observation-based estimates of $\langle \boldsymbol{u}_H \rangle$ at the Earth's core surface range from 4–22 km yr^{-1}.

The spread in the values reported in Table 1 is a consequence both of the different geomagnetic observations used, and of the different methods of flow estimation employed. All previous estimates of $\langle \boldsymbol{u}_H \rangle$ suffer from a number of fundamental limitations. First, as mentioned above, flow along contours of B_r at the core surface produces no SV (Backus 1968; Backus & LeMouël 1986) so this flow component is unconstrained by magnetic observations. Secondly, small scales of the MF and SV cannot be resolved in present geomagnetic field models, limiting flow inversions to large scales (Hulot *et al.* 1992). Moreover, large-scale SV can be generated by the interactions of small-scale field and large-scale flow, or large-scale field and small-scale flow (Bullard & Gellman 1950), so core flow models based only on the observed MF and SV may be biased (Eymin & Hulot 2005; Gillet *et al.* 2009). Finally, the influence of magnetic diffusion is almost always ignored in inversion schemes which may lead to local biases in the flow determination (Amit & Christensen 2008). These difficulties have been well illustrated in studies of core flow inversions of the output from numerical dynamo models. Rau *et al.* (2000) found that the mean core surface flow magnitude obtained by inversion underestimated the true surface flow magnitude by as much as a factor of 2 (see their table 2) even if information concerning all length scales of the core surface MF is provided. The magnitude estimates of Amit *et al.* (2007) using their helical flow inversion method are better, typically within about ±15 per cent of the true rms flow magnitude, but when the SV was low-pass filtered, removing the small-scale details, their estimates also deteriorated significantly.

Uncertainties related to existing core flow magnitude estimates motivate us to explore a new alternative scheme. The approach set out below allows one to estimate the rms core surface flow magnitude $\langle \boldsymbol{u}_H \rangle$ from knowledge of spatial spectra of MF and SV at a particular epoch together with prior knowledge on field-flow alignment obtained from numerical dynamo models. We argue below that global aspects of this essential facet of magnetic induction are adequately captured in the present generation of numerical dynamo models.

Knowledge concerning the relative alignment of magnetic field and flow in rapidly rotating, convection-driven, dynamos is central to our approach. Field-flow alignment, how it arises dynamically (Mason *et al.* 2006), its relation to dynamo saturation (Cameron & Galloway 2006; Cattaneo & Tobias 2009; Schrinner *et al.* 2010) and its influence on the partitioning between kinetic and magnetic energies (Archontis *et al.* 2007) are subjects of ongoing debate among dynamo theoreticians. It is also intimately related to an integral property called cross-helicity (Moffatt 1978), which is of great interest in studies of magnetohydrodynamic (MHD) turbulence (Perez & Boldyrev 2007) where problems are formulated in terms of the Elsasser variables ($\boldsymbol{u} \pm \boldsymbol{B}$) (Elsasser 1950b). To our knowledge the only previous study of field-flow alignment in numerical models of the geodynamo was that by Takahashi & Matsushima (2005). They observed that as the convective forcing (measured by the Rayleigh number Ra) was increased, less flow perpendicular to field lines occurred, the dynamos became less efficient, and there was a reduction in magnetic energy. In this investigation we focus on field-flow alignment close to the outer boundary and on extracting the information required by our flow magnitude estimation scheme. We study the relation between different characteristic field structures and the degree of field-flow alignment. We also investigate the dependence of the globally averaged amount of field-flow alignment close to the outer boundary on the non-dimensional parameters controlling the numerical dynamo models.

In Section 2 we present the mathematical details of our new flow magnitude estimation scheme; the information required is shown to take the form of MF and SV spectra together with an rms measure of the field-flow alignment at the core surface. In Section 3 we test the method using a small suite of numerical dynamo models, and propose a scaling law for applying it to the Earth's core. We also present spatial variations of field-flow alignment in the models and discuss the underlying mechanisms at work. In Section 5 we apply our scheme to the Earth, using both recent and historical geomagnetic field models, and derive new estimates for $\langle \boldsymbol{u}_H \rangle$ in the Earth's core and how this has varied with time. The impact of unobserved small scales on estimates of $\langle \boldsymbol{u}_H \rangle$ is discussed and a new range of plausible values is proposed.

In Section 6 we report new estimates of Rm and Ro based on our results. Flow magnitude estimates based on the observed MF and SV, and also estimates taking into account possible extrapolations to smaller scales are considered. In the calculation of Ro we assign flow length scales $\mathcal{L}_u$ based on the SV spectrum. In addition to the traditional Rm $= \mathcal{U}\mathcal{L}_B^h/\eta$, we consider an alternative magnetic Reynolds number Rm$_r = \mathcal{U}(\mathcal{L}_B^r)^2/\eta\mathcal{L}_B^h$ that takes into account radial magnetic diffusion. Here $\mathcal{L}_B^h$ is the length scale of the MF in the horizontal direction while $\mathcal{L}_B^r$ is the length scale of the MF in the radial direction, associated with a magnetic diffusion boundary layer close to the core surface. A magnetic Reynolds number containing two distinct length scales was previously proposed by Takahashi & Matsushima (2005) and Takahashi *et al.* (2008). Their analysis focused on comparing the importance of stretching of MF by the flow to the effects of magnetic diffusion, that is, they instead accounted for distinct flow and field length scales. In contrast, we consider the importance of horizontal advection

Table 1. Estimates of the core surface flow magnitude $\langle u_H \rangle$ in units of km yr^{-1} from a selection of previous studies. Flow magnitudes have been rounded to 2 significant figures for easy comparison. Ranges quoted correspond to different magnetic field models, physical assumptions, parametrizations and inversion strategies explored in the flow estimation for each study. Methods are reported in terms of the categories INV indicating rms values from full inversions of the frozen-flux radial induction equation, PE indicating rms point estimates of the flow normal to null flux curves and TF indicating tracking of individual non-dipole field features. In the data column names of field models are given where available, otherwise a reference is provided.

Study	Data	Epoch	Method	$\langle u_H \rangle$/km yr^{-1}
Lesur *et al.* (2010)	Co-estimated from CHAMP data	2005	INV	$11 - 13$
Gillet *et al.* (2009)	*CM4 / xCHAOS*	1960–2007	INV	$12 - 14$
Olsen & Mandea (2008)	*xCHAOS*	2000–2007	INV	$10 - 17$
Wardinski *et al.* (2008)	*CHAOS*	2000–2006	INV	$16 - 18$
Pais & Jault (2008)	*CHAOS*	2001–2004	INV	$16 - 19$
Whaler & Holme (2007)	*ufm1*	1970–1980	PE	$16 - 19$
Amit & Olson (2006)	*gufm1*	1840–1990	INV	$8 - 15$
Amit & Olson (2004)	Langlais *et al.* (2003)	1980–2000	INV	$7 - 22$
Pais *et al.* (2004)	*ufm1*	1840–1990	INV	$4 - 12$
Jackson (1997)	*ufm1*	1840–1990	INV	$11 - 19$
Backus *et al.* (1996)	*IGRF1980*	1980	PE	13
Bloxham (1992)	*ufm1*	1840–1990	INV	$10 - 13$
Gire & LeMouël (1990)	*USGS80, GSFC80*	1980	INV	15
Bloxham (1989)	Bloxham & Jackson (1989)	1915–1980	INV	$11 - 19$
Voorhies (1986)	*GSFC80*	1960–1980	INV	$9 - 22$
Booker (1969)	*GSFC(12/66)*	1945–1960	PE	9
Kahle *et al.* (1967b)	Vestine *et al.* (1947);	1912–1955	INV	$10 - 15$
	Nagata & Syono (1961)	1955–1960		
Bullard *et al.* (1950)	Vestine *et al.* (1947)	1905–1945	TF	$8 - 14$

compared to radial magnetic diffusion by using distinct radial and horizontal MF length scales. We evaluate Ro, Rm and Rm$_r$ for various possible choices of $\mathcal{L}_u$ and $\mathcal{L}_B^h$. Limitations of the new methodology are also discussed. In Section 7 we conclude with a summary of our findings, describe possible extensions to other MHD systems and discuss implications for the geodynamo.

2 THEORY

The radial magnetic induction equation in spherical polar coordinates (r, θ, ϕ) just below an impenetrable boundary where the radial velocity vanishes ($u_r = 0$) takes the form

$$\frac{\partial B_r}{\partial t} + \boldsymbol{u_H} \cdot \boldsymbol{\nabla_H} B_r + B_r(\boldsymbol{\nabla_H} \cdot \boldsymbol{u_H}) = \eta \left[\frac{1}{r^2} \frac{\partial^2}{\partial r^2}(r^2 B_r) + \boldsymbol{\nabla_H}^2 B_r \right], \tag{1}$$

where η is magnetic diffusivity and $\boldsymbol{\nabla_H} = \boldsymbol{\nabla} - (\partial/\partial r)\hat{\mathbf{r}}$ is the gradient tangential to the spherical surface. The frozen-flux hypothesis (Roberts & Scott 1965; Jackson & Finlay 2007) assumes that the majority of SV on short time-scales and large length scales is produced by the advection and stretching action of the velocity field rather than diffusion of the magnetic field due to the finite electrical conductivity. Under this assumption, (1) simplifies to

$$\frac{\partial B_r}{\partial t} + \boldsymbol{u_H} \cdot \boldsymbol{\nabla_H} B_r + B_r(\boldsymbol{\nabla_H} \cdot \boldsymbol{u_H}) = 0. \tag{2}$$

We further assume that purely toroidal flow with $\boldsymbol{\nabla_H} \cdot \boldsymbol{u_H} = 0$ is responsible for the majority of the observed SV. Whaler (1980) argued that extreme points where $\boldsymbol{\nabla_H} B_r = 0$ are characterized by low SV, suggesting that poloidal motions at these locations are weak. Lloyd & Gubbins (1990) later carried out successful inversions for purely toroidal core flows arguing that this is the most sensible zeroth order approximation, especially given the difficulty in constraining poloidal flows with SV. Even when alternative assumptions such as tangential geostrophy (LeMouël 1984) or helical flow (Amit & Olson 2004) are made, the inverted flows are usually predominantly toroidal. For example, Bloxham (1992) found that in his tangentially geostrophic steady flows, spanning 1840–1990,

toroidal motions accounted for over 90 per cent of the kinetic energy; more recently Wardinski *et al.* (2008) found that toroidal flows constituted 93 per cent of the kinetic energy of their tangentially geostrophic time-dependent flows derived from a field model based on satellite observations. The dominance of toroidal over poloidal flows can also be seen in the kinetic energy spectra of Eymin & Hulot (2005, their fig. 4b) and Pais & Jault (2008, their fig. 6). Furthermore, in the study of numerical dynamos models by Rau *et al.* (2000) toroidal flows were found to account for more than 90 per cent of the total kinetic energy close to the outer boundary. Although weak poloidal flow likely exists at the core surface (Beggan & Whaler 2008), focusing on toroidal flows is probably a reasonable simplifying approximation, especially in the context of global flow magnitude estimates.

Under the toroidal flow assumption, the radial frozen-flux induction eq. (2) simplifies to

$$\frac{\partial B_r}{\partial t} = -\boldsymbol{u_H} \cdot \boldsymbol{\nabla_H} B_r. \tag{3}$$

Next, since we perform global averaging, so it is convenient to introduce a bracket notation to represent the rms value of any scalar quantity g on a spherical surface S of radius $r = c$

$$\langle g \rangle = \sqrt{\frac{1}{4\pi} \int_S [g(c)]^2 \ \sin\theta \, \mathrm{d}\theta \, \mathrm{d}\phi}. \tag{4}$$

Applying this averaging operator to both sides of (3) we obtain,

$$\langle \partial B_r / \partial t \rangle = \langle \boldsymbol{u_H} \cdot \boldsymbol{\nabla_H} B_r \rangle. \tag{5}$$

The scalar product on the right-hand side of (5) can be expanded as,

$$\langle \partial B_r / \partial t \rangle = \langle |\boldsymbol{u_H}| \, |\boldsymbol{\nabla_H} B_r| \, |\cos\gamma| \rangle, \tag{6}$$

with

$$\cos\gamma = \frac{\boldsymbol{u_H} \cdot \boldsymbol{\nabla_H} B_r}{|\boldsymbol{u_H}| \, |\boldsymbol{\nabla_H} B_r|}, \tag{7}$$

where γ is the angle between the vectors $\boldsymbol{u_H}$ and $\boldsymbol{\nabla_H} B_r$ so that

$(\pi/2 - \gamma)$ is the angle between a B_r–contour and the core surface flow $\boldsymbol{u}_H$. Note that $\cos\gamma\,(\theta,\phi)$ is a local scalar quantity, for which the rms on a spherical surface may be calculated in the usual manner.

To make further progress, an additional step is required. We proceed assuming that $|\boldsymbol{u}_H\,(\theta,\phi)|$, $|\boldsymbol{\nabla}_H\,B_r(\theta,\phi)|$ and $|\cos\gamma\,(\theta,\phi)|$ are spatially uncorrelated, which makes it possible to separate the rms of their product into the product of their respective rms values.

$$\langle|\boldsymbol{u}_H||\boldsymbol{\nabla}_H B_r||\cos\gamma|\rangle = \langle\mathbf{u_H}\rangle\,\langle\boldsymbol{\nabla}_H B_r\rangle\,\langle\cos\gamma\rangle, \qquad (8)$$

where we have been able to dispense with the absolute signs on the right-hand side because $|g|^2 = g^2$. We are unable to justify the assumption of spatially uncorrelated quantities in (8) *a priori*, but by analysing the output from numerical dynamos models we have found that empirically this is often the case (see Section 3). A related assumption was previously made by Hulot *et al.* (1992) in their study of the effects of field truncation on the flow. They considered that the spectral coefficients representing the field and flow were independent, zero mean, random variables which enabled useful expressions for rms interaction terms to be obtained (see their section 4.2 and especially eq. 31b). It is worth recalling that our treatment does, of course, account for the directional correlation between the vector quantities $\boldsymbol{u}_H$ and $\boldsymbol{\nabla}_H\,B_r$ through the factor $\cos\gamma$ in the expansion of the scalar product; it is only the magnitudes of these two vector quantities and the magnitude of the cosine of the angle between them that we assume to be spatially uncorrelated.

Substituting (8) into (6) and rearranging gives

$$\langle\boldsymbol{u}_H\rangle = \frac{\langle\partial B_r/\partial t\rangle}{\langle\boldsymbol{\nabla}_H B_r\rangle\,\langle\cos\gamma\rangle}. \qquad (9)$$

This relation may easily be interpreted physically; it states that the rms flow magnitude is proportional to the rms magnitude of the SV and inversely proportional to the rms magnitude of the horizontal gradient of the radial field (with a large gradient even a weak flow can produce large SV). It also clearly reveals that if the flow is on average nearly parallel to contours of the radial field (i.e. $\langle\cos\gamma\rangle \sim 0$) then a very strong flow will be necessary to explain the observed SV.

Considering the velocity and magnetic fields output from numerical dynamo models on a latitude–longitude grid, one can directly estimate the quantities in (9), $\boldsymbol{\nabla}_H B_r$, $\partial B_r/\partial t$ as well as $\cos\gamma$, in physical space. In Section 3, quantities that involve spatial derivatives (such as $\boldsymbol{\nabla}_H B_r$) are calculated using centred finite-differencing on the same grid that was used for the dynamo calculations. The rms quantities are then be calculated by a numerical approximation to (4).

Alternatively, $\langle\partial B_r/\partial t\rangle$ and $\langle\boldsymbol{\nabla}_H B_r\rangle$ can be calculated directly in spectral space by summing appropriate combinations of spherical harmonics. This turns out to be particularly useful when working with observation-based field models where the MF and SV are typically provided in the form of spherical harmonic coefficients (see Section 5). As shown in the Appendix, (9) can be written in terms of Schmidt quasi-normalized spherical harmonic spectra as

$$\langle\boldsymbol{u}_H\rangle = \frac{\sqrt{\sum\limits_{l=1}^{\infty}\frac{(l+1)}{(2l+1)}Q_l(c)}}{\sqrt{\sum\limits_{l=1}^{\infty}\frac{l(l+1)^2}{c^2(2l+1)}R_l(c)}\,\langle\cos\gamma\rangle}, \qquad (10)$$

where l is the spherical harmonic degree, and $R_l(c)$ and $Q_l(c)$ are Mauersberger–Lowes spectra (Mauersberger 1956; Lowes 1966; Lowes 1974) of the MF and the SV, respectively, at the core surface, as defined in the Appendix. Since (10) is written in terms of the

spherical harmonic spectra, it is evident that our estimate of $\langle\boldsymbol{u}_H\rangle$ uses only information concerning the globally averaged properties of the field and is not based on any particular local features, since all phase information is absent. In the next section we use numerical dynamo models to test this flow estimation scheme.

3 TESTS WITH NUMERICAL DYNAMO MODELS

3.1 Setup and non-dimensional parameters for numerical experiments

In this section we report a series of synthetic tests of the method proposed in the previous section. These tests involve 3-D numerical dynamo models computed using the simulation code MAGIC (Wicht 2002). We use an earth-like geometry of $r_i/r_o = 0.35$, where r_i is the inner boundary radius and r_0 is the radius of the outer boundary. We examined models sampling a range of control parameters in an attempt to characterize the parameter dependence of our results. All the models studied have electrically insulating, no-slip and isothermal (fixed temperature) boundary conditions. In all cases a spherical harmonic truncation degree of 64 was employed except in case M8 where it was increased to 168. The same truncation level was used for both the field and the flow. In physical space the grid is regular in the horizontal direction, that is, fixed angular grid step in both longitude and latitude, with 192 longitude grid points and 96 latitude grid points for all cases except M8 which used 480 and 240 points, respectively. The number of radial grid points increases with decreasing Ekman number so that each model has at least five grid points resolving the Ekman boundary layers. Because we are mostly interested in magnetic field evolution on time-scales short compared to the magnetic diffusion time, and because we will later apply our method to observations of the geomagnetic field, we focused on dipole-dominated non-reversing dynamos.

The control parameters, the Ekman number $\mathrm{Ek} = \nu/\Omega D^2$, the Rayleigh number $\mathrm{Ra} = \alpha g_0\Delta T D^3/\kappa\nu$, the Prandtl number $\mathrm{Pr} = \nu/\kappa$ and the magnetic Prandtl number $\mathrm{Pm} = \nu/\eta$, for the runs investigated are given in Table 2. Here α is the thermal expansivity, g_0 is the value of gravity on the outer boundary, ΔT is the temperature difference between the inner and outer boundaries, D is the shell thickness, ν is the kinematic viscosity, κ is the thermal diffusivity, Ω is the rotation rate and η is as before the magnetic diffusivity. The suite of models studied here is the same as that previously studied by Amit & Christensen (2008) with the addition of one extra model with lower magnetic Prandtl number (model M9 in Table 2). Also given in Table 2 are the diagnostic output values of the global magnetic Reynolds number $\mathrm{Rm} = \mathcal{U}D/\eta$ and the global Rossby number $\mathrm{Ro} = \mathcal{U}/\Omega D$ calculated using $\mathcal{U}$ based on the total kinetic energy in the spherical shell and a single length scale D. The models differ in the complexity of the small-scale features, that is, by the amount of kinetic energy which is accommodated by the small scales. Due to numerical limitations, all the models explored here are unfortunately many orders of magnitude away from the Earth-like values of Ra, Ek and Pm. They do however have the correct order of magnitude for the global magnetic Reynolds number, which suggests they may correctly mimic kinematic and induction processes relevant to the Earth's core.

We also report the value of an additional parameter, which we term the 'magnetic modified Rayleigh number',

$$\mathrm{Ra}_\eta = \frac{\alpha g_0\Delta T D}{\eta\Omega} = \frac{\mathrm{Ra}\cdot\mathrm{Ek}\cdot\mathrm{Pm}}{\mathrm{Pr}} = \mathrm{Ra}'\cdot\mathrm{Pm}, \qquad (11)$$

Table 2. Input control parameters for the numerical dynamos and estimated values for Earth's core: Rayleigh number Ra, Ekman number Ek, magnetic Prandtl number Pm and Prandtl number Pr (see text for definitions). Also given are the model outputs Rm and Ro and a new non-dimensional parameter Ra_η that we term the magnetic modified Rayleigh number. All estimates for the Earth's core are from Christensen & Aubert (2006) except Rm from Bloxham & Jackson (1991).

Case	Ra	Ek	Pm	Pr	Rm	Ro	Ra_η
$M1$	3×10^5	10^{-3}	4	1	110	2.75×10^{-2}	1200
$M2$	1.5×10^6	3×10^{-4}	2	1	96	1.44×10^{-2}	900
$M3$	3×10^6	3×10^{-4}	3	1	296	2.96×10^{-2}	2700
$M4$	8×10^6	2×10^{-4}	3	1	487	3.25×10^{-2}	4800
$M5$	1.5×10^7	1×10^{-4}	2	1	329	1.65×10^{-2}	3000
$M6$	8×10^6	1×10^{-4}	2	1	177	8.85×10^{-3}	1600
$M7$	1.5×10^7	1×10^{-4}	4	1	617	1.54×10^{-2}	6000
$M8$	1.2×10^8	3×10^{-5}	2.5	1	876	1.05×10^{-2}	9000
$M9$	7.5×10^6	2×10^{-4}	0.5	1	51	2.04×10^{-2}	375
Earth	10^{23}	5×10^{-15}	2×10^{-6}	0.25	500	6×10^{-6}	4000

Table 3. $\langle \cos \gamma \rangle$ and the ratio $\langle u_H \rangle^{\text{cal}} / \langle u_H \rangle^{\text{tr}}$ at the top of the free stream of the numerical dynamos. $\langle u_H \rangle^{\text{cal}}$ is the value computed using scheme (9) and $\langle u_H \rangle^{\text{tr}}$ is the true core surface flow from the dynamo model. The range, mean (μ) and standard deviation (σ) from 10 arbitrarily sampled snapshots are given for both quantities.

Case	$\langle \cos \gamma \rangle$			$\langle u_H \rangle^{\text{cal}} / \langle u_H \rangle^{\text{tr}}$		
	Range	μ	σ	Range	μ	σ
$M1$	$0.607 - 0.652$	0.633	0.013	$0.784 - 0.981$	0.849	0.065
$M2$	$0.615 - 0.645$	0.628	0.008	$0.822 - 1.273$	0.962	0.127
$M3$	$0.653 - 0.666$	0.661	0.004	$0.801 - 0.971$	0.902	0.051
$M4$	$0.670 - 0.685$	0.677	0.005	$0.930 - 1.085$	0.985	0.042
$M5$	$0.662 - 0.671$	0.667	0.003	$0.879 - 1.061$	0.989	0.050
$M6$	$0.636 - 0.653$	0.644	0.005	$0.916 - 1.277$	1.026	0.097
$M7$	$0.673 - 0.688$	0.681	0.005	$0.893 - 1.055$	1.002	0.045
$M8$	$0.661 - 0.671$	0.667	0.003	$0.877 - 1.039$	0.951	0.047
$M9$	$0.627 - 0.655$	0.641	0.009	$1.145 - 1.439$	1.319	0.090

where $Ra' = Ra \cdot Ek/Pr$ is the modified Rayleigh number often employed in studies of rotating convection (see, e.g. Olson *et al.* 1999; Christensen *et al.* 2001). Physically, the traditional Rayleigh number, Ra, measures the competition between buoyancy forces resulting from a temperature (and hence density) difference, and the dissipative effects of viscosity and thermal conduction. However, in the MHD environment of the geodynamo, viscosity is expected to be weak in the bulk of the fluid where strong magnetic fields are also present. In this scenario a moving fluid parcel will dissipate energy not through the familiar viscous effects but through the electrical currents and concommittant Ohmic dissipation produced as it distorts magnetic field lines; conduction of heat on the other hand continues to play a similar role as before. It thus seems intuitively reasonable that a magnetic modified Rayleigh number Ra_η, which is the modified Rayleigh number Ra' with ν replaced by η (in analogy to the magnetic Reynolds number where ν is replaced by η compared to the hydrodynamic Reynolds number), will be of relevance in rapidly rotating, convection-driven dynamos.* We will show later that Ra_η turns out to be very useful when investigating the average amount of field-flow alignment and that it may be related to the efficiency of induction in numerical dynamo models.

---

* Note that Ra_η also arises naturally when one assumes a balance between Coriolis and buoyancy forces in the Navier–Stokes equation and an advection–diffusion balance in the induction equation, thus it appears to be rather fundamental to the saturated state in rapidly rotating, convection-driven dynamos.

3.2 Synthetic tests of flow magnitude estimation scheme

One important step in the scheme outlined in Section 2 was the assumption that the magnitudes $|\mathbf{u_H}|$, $|\nabla_H B_r|$ and $|\cos \gamma|$ are spatially uncorrelated. Before proceeding further, we first examined this assumption with our suite of numerical dynamos. The correlation coefficient (see, e.g. Rau *et al.* 2000) was computed between the three pairs of scalar functions for each dynamo case, for each of 10 arbitrarily sampled snapshots. We found that the correlation coefficients between the fields were usually low, indicating that our assumption that these fields are uncorrelated is an acceptable approximation.

Next we applied our flow magnitude estimation scheme (9) to the dynamo models described in Table 2. $\langle \cos \gamma \rangle$ can be directly obtained in numerical dynamos by calculating the rms value of $\cos \gamma(\phi, \theta)$ on a spherical surface just below the outer Ekman–Hartmann boundary layer. These calculations were carried out on the numerical grid used for the dynamo modelling. 10 arbitrary snapshots were used in each case to obtain the range, time-average and standard deviation measures for each dynamo model. The results are summarized in Table 3. A typical value of $\langle \cos \gamma \rangle \sim 0.65$ corresponds to an angle $\gamma \sim 50°$ between $\boldsymbol{u_H}$ and $\nabla_H B_r$ or to an angle of $\sim 40°$ between the velocity vector and a B_r-contour.

Once $\langle \cos \gamma \rangle$ had been estimated, the validity of the flow magnitude estimation scheme was assessed using the synthetic SV produced by the numerical dynamos. This series of experiments tests whether, despite the assumptions and approximations being made, the method is capable of producing useful flow magnitude estimates. In each dynamo model snapshot we evaluated the rms values
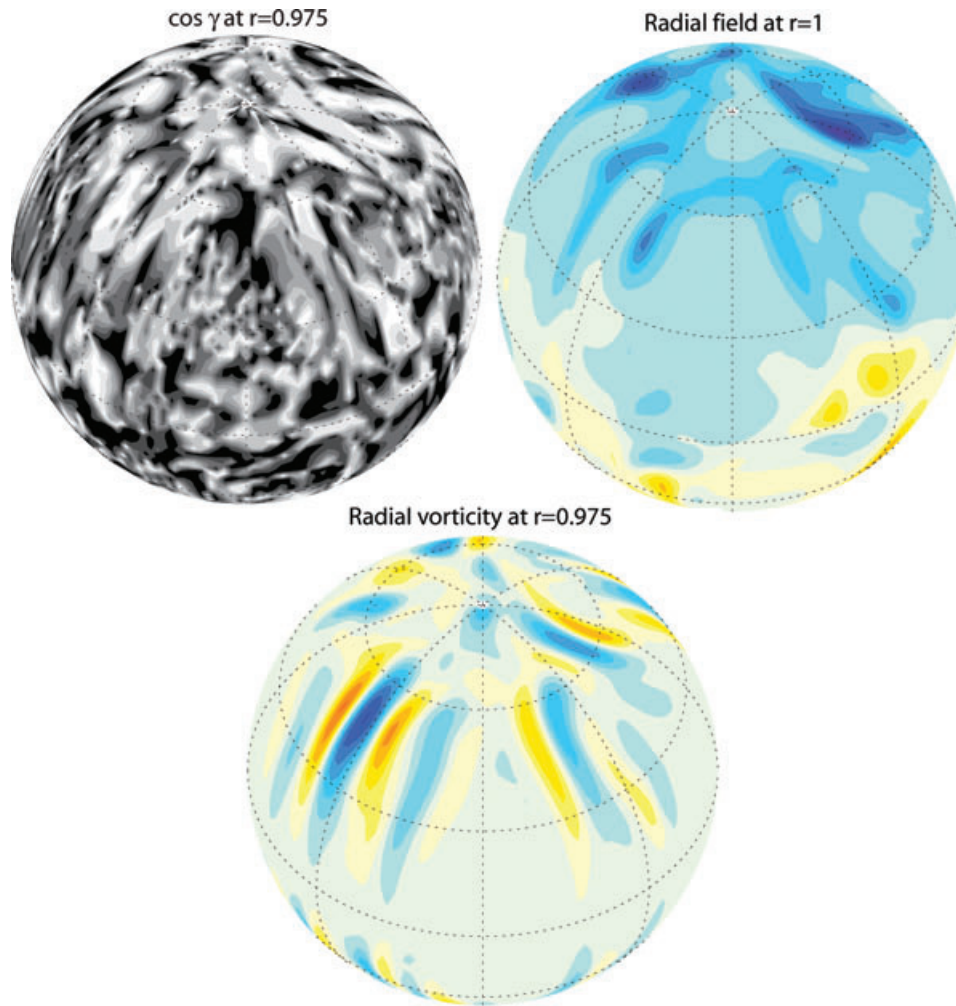
Figure 1. Spatial distribution of $|\cos\gamma|$ from a snapshot of case $M2$ at the top of the free stream, values close to 0 are white while values close to 1 are black, (top left panel); radial magnetic field at the outer boundary (top right panel); and radial vorticity at the top of the free stream (bottom panel). All maps are centred at $\phi = 0°$.

$\langle \partial B_r / \partial t \rangle$ and $\langle \nabla_H B_r \rangle$ at the top of the free stream. Then, using the value of $\langle \cos\gamma \rangle$ for that snapshot, we applied (9) to find the 'calculated' magnitude of the horizontal velocity $\langle \boldsymbol{u}_H \rangle^{\mathrm{cal}}$ and compared this with the rms value of the 'true' horizontal velocity $\langle \boldsymbol{u}_H \rangle^{\mathrm{tr}}$. The deviation of the ratio $\langle \boldsymbol{u}_H \rangle^{\mathrm{cal}} / \langle \boldsymbol{u}_H \rangle^{\mathrm{tr}}$ from unity quantifies the error due to the approximations made in the flow estimation method.

The results of these tests are reported in Table 3. The errors in the flow magnitudes detailed there quantify the combined influence of failure of the frozen-flux assumption, the presence of poloidal flows and departures from the assumption that the magnitudes of $|\mathbf{u_H}|$, $|\nabla_H B_r|$ and $|\cos\gamma|$ are uncorrelated. The average difference between $\langle \boldsymbol{u}_H \rangle^{\mathrm{tr}}$ and $\langle \boldsymbol{u}_H \rangle^{\mathrm{cal}}$, over all the cases studied, is 7.9 per cent; in individual cases this difference varies from 0.2–32 per cent. The generally good agreement between the true and calculated flow magnitudes is very encouraging. Note that the results presented in Table 3 are generally better than those achieved for the retrieval of rms flow magnitude by conventional inversion schemes that were previously tested on dynamo simulations (Rau *et al.* 2000; Amit *et al.* 2007). On the basis of Table 3 we would expect (9) to yield a flow magnitude estimate within 8 per cent of the true value, assuming $\langle \cos\gamma \rangle$ along with the MF and its SV are perfectly known; of course in reality these conditions will not be satisfied and larger errors should be expected.

4 FIELD-FLOW ALIGNMENT IN NUMERICAL DYNAMO MODELS

4.1 Spatial distribution and physical significance of $|\cos\gamma|$

Local alignment between the magnetic fields and the flow in numerical models of the geodynamo was previously studied by Takahashi & Matsushima (2005). Given its central role in our scheme, and its potential relevance to the dynamo saturation mechanisms (Cameron & Galloway 2006), we investigate here spatial variations of $|\cos\gamma|$ and discuss the insights provided concerning induction processes at the core surface.

In Fig. 1 we present a map of $|\cos\gamma(\theta, \phi)|$ just below the outer Ekman–Hartmann boundary layer in a snapshot from a relatively large-scale numerical dynamo (case $M2$). This case is representative of the main features found in other models which possess more complex small-scale field and flow structures. We also present the radial magnetic field at the outer boundary and the radial vorticity just below the boundary layer. High-latitude intense flux patches maintained by cyclonic flow structures are in general associated with low values of $|\cos\gamma|$, that is, low efficiency of induction, whereas low-latitude field structures are often associated with higher values of $|\cos\gamma|$ and thus higher efficiency of induction. Zooming
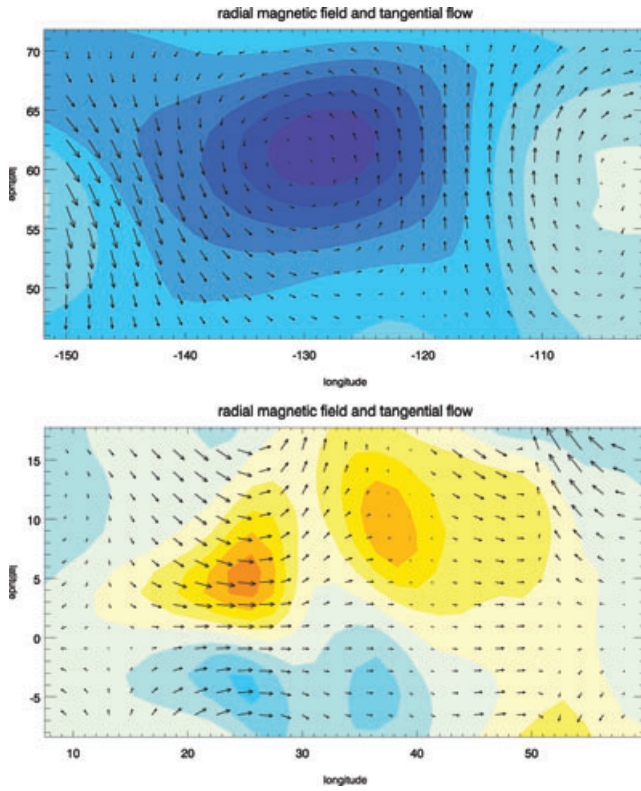
Figure 2. Zoom into a regions of low $|\cos\gamma|$ (top panel) and high $|\cos\gamma|$ (bottom panel) from Fig. 1. Radial magnetic field (colours) and horizontal flow (arrows) are shown.

into each of these structures reveals further details. In Fig. 2(a) we find low values of $|\cos\gamma|$ at a high-latitude region where a columnar flow structure, resulting from convection under the influence of rapid rotation, intersects the outer boundary. Cyclonic, columnar flows involve downwelling close to the outer boundary (Olson *et al.* 1999; Olson *et al.* 2002) with converging flow that concentrates radial field into characteristic intense flux bundles at the outer boundary (Gubbins *et al.* 2000; Olson & Christensen 2002). In these intense field structures, contours of B_r are nearly parallel to $\mathbf{u_H}$ thus leading to low values of $|\cos\gamma|$. In Fig. 2(a), we observe that the toroidal flow is mostly around the flux bundle, almost

parallel to B_r-contours. In contrast, considering Fig. 2(b), at low- and mid-latitudes magnetic field structures drift with the large-scale predominantly zonal flow. For these structures the toroidal flow is often perpendicular to B_r-contours, yielding large local $|\cos\gamma|$ values. The nearly perpendicular relation between $\mathbf{u_H}$ and B_r-contours in Fig. 2(b) is particularly evident at the two intense patches centred at $\sim 25°$E.

In Fig. 3 we present a histogram showing the distribution of $|\cos\gamma(\theta, \phi)|$ calculated at the dynamo model collocation grid points; the sign of $\cos\gamma(\theta, \phi)$ is of course irrelevant to the rms value $\langle\cos\gamma\rangle$. This distribution is certainly not uniform, as might naively have been expected if $|\cos\gamma(\theta, \phi)|$ was assumed to be a random variable. Instead it shows two peaks, one at $|\cos\gamma| \sim 0$ (horizontal flow parallel to contours of B_r), the other at $|\cos\gamma| \sim 1$ (horizontal flow perpendicular to contours of B_r). The distribution is characterized by lower occurrences for intermediate $|\cos\gamma|$. In this dynamo, for a large fraction of the core surface the field and flow are in good alignment and hence induction is weak, see for example, Fig. 2(a). In addition, there is a significant region where the field and flow are nearly perpendicular and significant induction takes place (as in Fig. 2b). It is the combined effect of regions with slow-evolving magnetic structures maintained by columnar convection (with nearly field-aligned flow contributing to low $|\cos\gamma|$), together with lower latitude regions where predominantly zonal flows act perpendicular to field patches (giving high $|\cos\gamma|$) that gives rise to the intermediate global values of $\langle\cos\gamma\rangle \sim 0.65$ reported in Table 3.

We suggest that the quantity $|\cos\gamma|$ is a useful local diagnostic of the induction process. Low $|\cos\gamma|$ corresponds to horizontal flow nearly parallel to contours of B_r and hence weak advective SV and inefficient induction, whereas high $|\cos\gamma|$ corresponds to flow nearly perpendicular to contours of B_r and efficient motional induction for a given magnitude of flow and field gradient. We therefore term $|\cos\gamma|$ the 'local induction efficiency', and $\langle\cos\gamma\rangle$ the 'global induction efficiency'.

The dynamo models presented here are in a regime where an α^2 dynamo mechanism operates (Olson *et al.* 1999). We find that consideration of the local efficiency of induction $|\cos\gamma|$ provides additional insight to the working of such dynamos. The low-latitude features are the surface manifestation of the strong stretching of poloidal field by radial outflow between a cyclone and an anti-cyclone. This is known to be a key ingredient in the α^2 dynamo
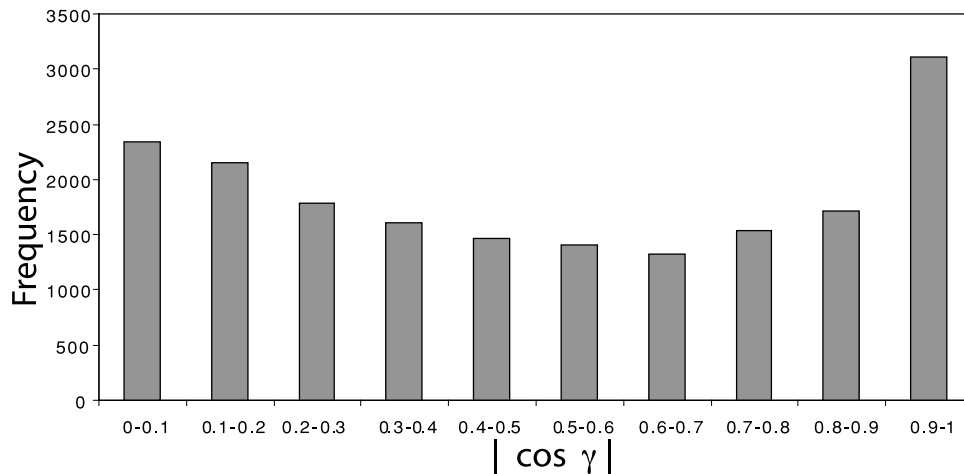
Figure 3. Histogram of $|\cos\gamma|$ from the same snapshot of $M2$ presented in Fig. 1. The histogram was constructed using all spatial grid points used in the dynamo calculation.
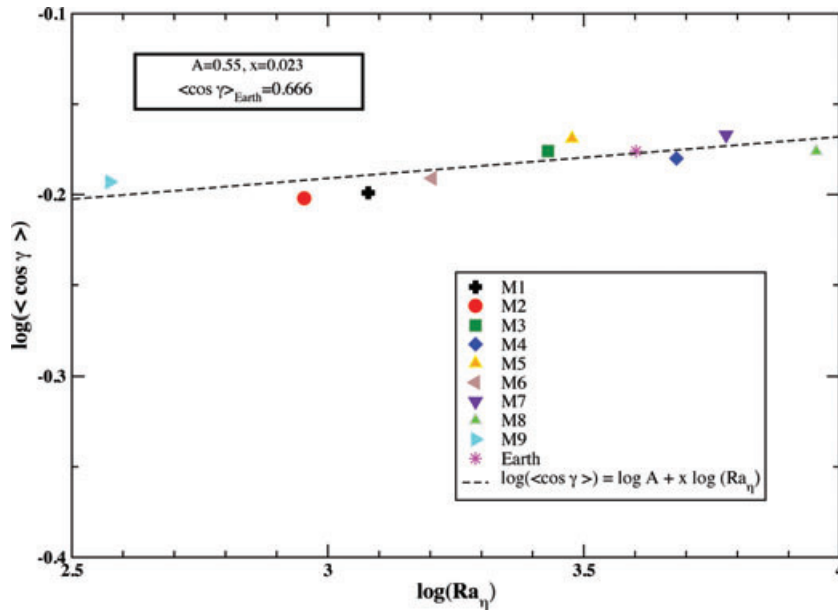
Figure 4. Power-law fit to $\langle \cos \gamma \rangle$ from the numerical dynamo models based on (13).

mechanism, see fig. 5 of Olson *et al.* (1999) and fig. 3(a) of Wicht & Tilgner (2010). The value of $|\cos \gamma|$ close to 1 associated with these features indicates efficient induction and marks their importance in the operation of the dynamo. In contrast the high-latitude cyclonic features possess low $|\cos \gamma|$ and perhaps indicate surface regions of importance for the saturation of the dynamo.

4.2 Parameter dependence and scaling of $\langle \cos \gamma \rangle$

To implement the proposed scheme for estimating the flow magnitude at Earth's core surface, we need to extrapolate $\langle \cos \gamma \rangle$ to the conditions pertaining to the core. In this section, we perform a power-law scaling analysis of $\langle \cos \gamma \rangle$ from our suite of numerical dynamo models to obtain the required estimate. Scaling approaches have previously been successfully applied for other global diagnostic properties of numerical dynamos (Christensen & Tilgner 2004; Christensen & Aubert 2006; Olson & Christensen 2006; Christensen 2010). Since Pr is thought to have a similar value in the numerical dynamo models and in the Earth's core, we consider the variation of $\langle \cos \gamma \rangle$ as a function of Ek, Ra and Pm, beginning with a general power law of the canonical form,

$$\langle \cos \gamma \rangle = C_1 \mathrm{Ra}^{x_1} \mathrm{Ek}^{x_2} \mathrm{Pm}^{x_3}, \tag{12}$$

where C_1 is a constant pre-factor and x_i are powers. The best fitting result gives small positive values (less than 0.1) for all three powers, indicating that $\langle \cos \gamma \rangle$ depends only very weakly on the control parameters. Furthermore, the similarity in the values of x_1, x_2 and x_3 suggests that the scaling may be governed by a simpler power law of the form,

$$\langle \cos \gamma \rangle = A(\mathrm{Ra}_\eta)^x \tag{13}$$

where Ra_η is the magnetic modified Rayleigh number (11) and A is a constant. The best least-squares fit using law (13) occurs with $A = 0.55$ and $x = 0.023$ (Fig. 4) and was found to be almost as successful a fit with the more general power law (12).

The physical implication of (13) is that the global efficiency of induction $\langle \cos \gamma \rangle$ is largely controlled by the magnetic modified Rayleigh number Ra_η. Recall that Ra_η is identical to the modified Rayleigh number Ra' except that magnetic diffusivity substitutes for

the viscosity. It therefore measures how strongly the system is being forced by convection (against the influence of rotation) compared to how rapidly energy can be lost by Ohmic dissipation. For the Earth's core $\mathrm{Ra}_\eta \sim 4000$ is well within the range we have explored with numerical dynamos (Table 2); this indicates that present numerical dynamo models may already capture in a reasonable manner the global efficiency of induction (degree of field-flow alignment) at their outer surface. The dependence on Ra_η furthermore suggests that a trade-off must exist between the effects of more vigorous convection and stronger magnetic diffusion as an earth-like regime is approached. The effect of stronger driving (which will increase Ra_η and hence increase $\langle \cos \gamma \rangle$) together with stronger magnetic dissipation (which will tend to decrease $\langle \cos \gamma \rangle$) are predicted to combine to produce moderately efficient global induction characterized by an intermediate value of $\langle \cos \gamma \rangle \simeq 0.65$, at least for dipole-dominated non-reversing dynamos of the type studied here. For the flow magnitude estimation scheme the most important aspect of (13) is that $\langle \cos \gamma \rangle$ depends only extremely weakly on Ra_η; this gives us hope that inferences from the numerical dynamos investigated here may provide useful prior information for estimates of the flow magnitude in the Earth's core.

Substituting the values of the control parameters expected for the Earth's outer core (see Table 2) into power law (13) leads to a predicted value of $\langle \cos \gamma \rangle \simeq 0.666$; this is shown in Fig. 4 as the pink star. Note that in the construction of our power law we did not impose that the value of $\langle \cos \gamma \rangle$ for the Earth's core must lie in the range 0–1. This was achieved naturally from the very weak dependence of $\langle \cos \gamma \rangle$ on the control parameters and the trade-off between increasing $\langle \cos \gamma \rangle$ with increasing Ra, and decreasing $\langle \cos \gamma \rangle$ with decreasing Pm towards earth-like conditions. Given the uncertainties in the control parameters for the Earth's core, and possible errors in the scaling law due to the small number of dynamo models studied, we henceforth adopt a (rather large) range $\langle \cos \gamma \rangle = 0.65 \pm 0.05$ as being appropriate for the Earth's core. Note that the standard deviations in Table 3 suggest variations of $\sim \pm 0.05$ are in any case associated with the time-dependence of the dynamo process, so consideration of a range of values $\langle \cos \gamma \rangle = 0.6$–$0.7$ seems prudent.

5 FLOW MAGNITUDE ESTIMATES AT EARTH'S CORE SURFACE

In this section we present results of the application of the scheme set out above to geomagnetic observations, and provide new estimates for the flow magnitude at Earth's core surface. We begin by applying the method to the large-scale MF and SV derived from high-quality observations performed by the Ørsted, CHAMP and SAC-C satellites as encapsulated by the *xCHAOS* model of Olsen & Mandea (2008). We also quantify how uncertainty in $\langle \cos \gamma \rangle$ affects our flow magnitude estimates. The method is next applied to the MF and SV between 1840 and 1990 from the field model *gufm1* of Jackson *et al.* (2000). This enables variations in the flow magnitude over the historical era to be determined. We conclude by exploring possible spectral extrapolations of the observed MF and SV which permit investigation of the influence of unobserved small scales on flow magnitude estimates.

5.1 Core flow magnitude estimates from the observed large-scale MF and SV

An estimate of the core flow magnitude is obtained using (10), the spectra of the MF, R_l and the spectra of the SV, Q_l, at the core surface from the *xCHAOS* model (Olsen & Mandea 2008) evaluated in epoch 2004.0. We truncate the field model at degree $L = 10$ because above this level there are discrepancies among core surface

SV models produced by different authors (Gillet *et al.* 2010), and because unwanted crustal field may already significantly contribute to the MF signal by degree $L = 12$. We also tested our scheme using the *GRIMM* field model (Lesur *et al.* 2008) also truncated at degree 10; the results obtained were essentially identical to those reported here. Fig. 5 shows B_r and $\partial B_r / \partial t$ from *xCHAOS* at the core surface in 2004.0 as used for the calculations reported here. Based on the estimate of $\langle \cos \gamma \rangle = 0.65$ from scaling law (13) applied to the Earth's core, we obtain the result $\langle u_H \rangle = 12.5$ km yr^{-1}, well within the range of conventional core flow magnitude estimates (see Table 1).

5.2 Impact of uncertainty in field-flow alignment factor $\langle \cos \gamma \rangle$

Fig. 6 shows how estimates of $\langle u_H \rangle$ derived from the *xCHAOS* MF and SV models in 2004.0 change as $\langle \cos \gamma \rangle$ varies. For the extreme (and physically implausible) but formally limiting case of a core surface flow that is everywhere perpendicular to B_r-contours, that is $\langle \cos \gamma \rangle = 1$, we obtain a lower bound for the large-scale flow magnitude of $\langle u_H \rangle = 8.15$ km yr^{-1}. This is a formal lower limit given the assumptions inherent in our method; however it is very unlikely that such extreme flow-field alignment exists in the Earth's core and none of the numerical dynamo models studied possess such a high $\langle \cos \gamma \rangle$ value.
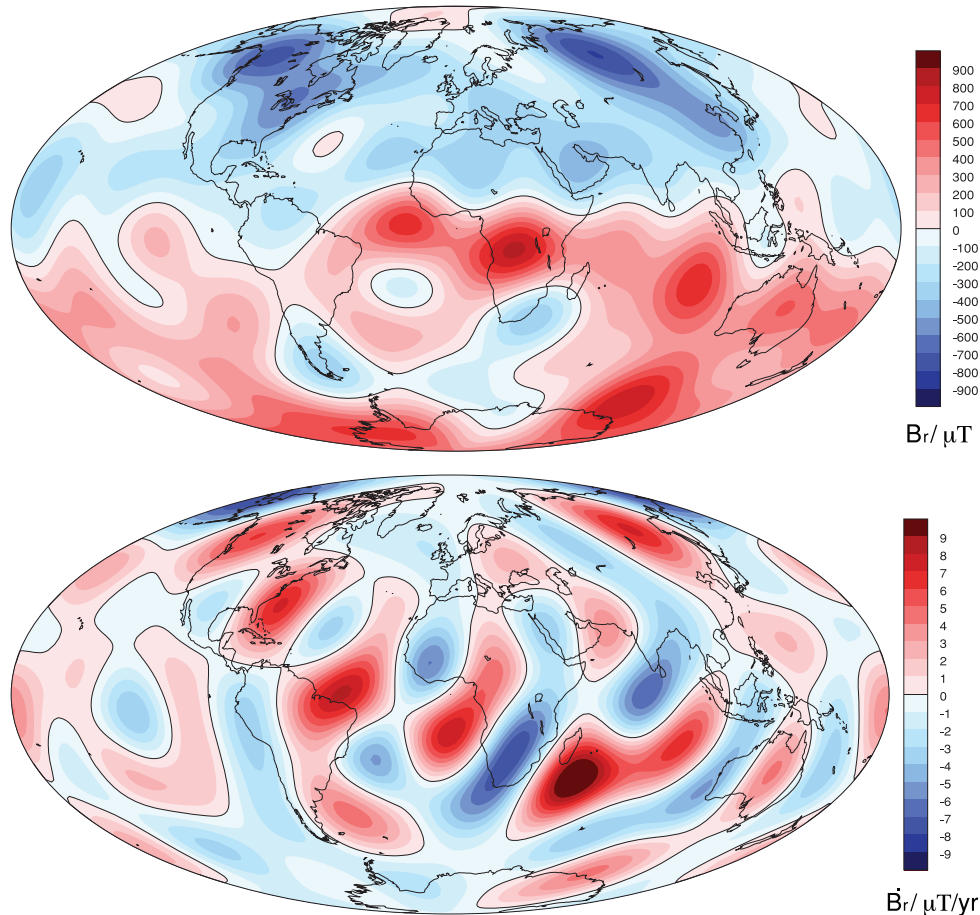
Figure 5. Radial magnetic field B_r in μT at the core–mantle boundary (top panel) and its secular variation $\partial B_r / \partial t$ in μT yr^{-1} (bottom panel) from the *xCHAOS* model of Olsen & Mandea (2008) in 2004.0 truncated at degree $L = 10$.
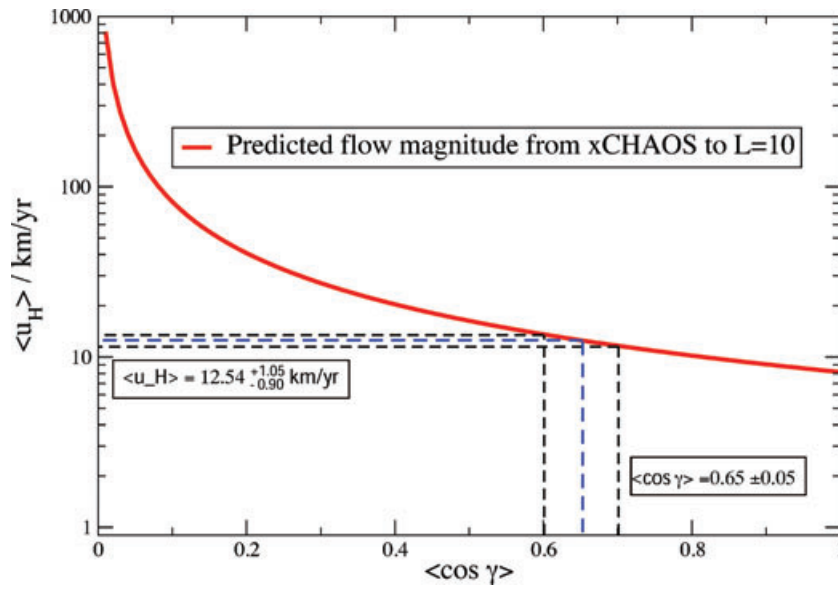
Figure 6. Variation of core surface flow magnitude $\langle \boldsymbol{u}_H \rangle$ determined from *xCHAOS* truncated at degree $L = 10$, as a function of $\langle \cos \gamma \rangle$.

In the opposite limit of horizontal flow along B_r-contours (field-aligned flow) for which $\langle \cos \gamma \rangle = 0$, there is a singularity in (10). Infinite $\langle \boldsymbol{u}_H \rangle$ is thus predicted if the flow were entirely along contours of B_r at the core surface. In that case no SV could be produced and all flow estimation methods based on frozen-flux inversion of SV will fail. However, a perfectly field-aligned flow also seems improbable and none of the numerical dynamo models we investigated suggest such a relation. Consideration of the range of $\langle \cos \gamma \rangle = 0.65 \pm 0.05$ leads to a range of core surface flow magnitudes $\langle \boldsymbol{u}_H \rangle$ of 11.6–13.6 km yr^{-1} (see Fig. 6). The very weak dependence of the result on the value of $\langle \cos \gamma \rangle$ gives confidence in the inferred flow magnitude.

5.3 Temporal variations in flow magnitude

To investigate temporal fluctuations in the rms flow magnitude, we applied our method to the *gufm1* historical core field model (Jackson *et al.* 2000) at yearly intervals between 1840.0 and 1990.0 with $\langle \cos \gamma \rangle = 0.65$. Fig. 7 shows the results with *gufm1* truncated at $L = 8$ and 10. For comparison we also present the rms flow variations determined by Amit & Olson (2006) using a full flow inversion of *gufm1* truncated at degree $L = 14$ (see the orange dashed line). Both techniques show similar variations in flow magnitude with the maximum amplitude occurring close to 1915. The same general pattern was also found by Jackson (1997) using his fully time-dependent, tangentially geostrophic flow inversion (see his fig. 4a).

It is noteworthy that the maximum in core flow magnitude in 1915 coincides with a maximum in the observed change in the length of day at the same time (see fig. 11 of Jackson 1997). Furthermore, the subsequent decrease in flow magnitude until around 1940, the increase from 1950 until 1970 and the weak decrease towards 1990 also follow the general trends in the observed change in the length of day over the past century (Jackson *et al.* 1993). The variations we find in flow magnitude are therefore qualitatively consistent with independent geodetic observations of the decadal changes of flow magnitude in the Earth's core. We therefore conclude that our approach is a feasible method for monitoring rms temporal
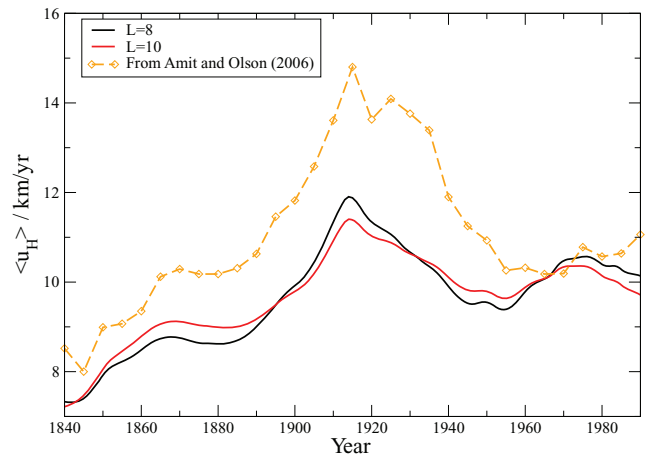
Figure 7. Core flow magnitude estimates based on the historical core field model *gufm1* (Jackson *et al.* 2000) between 1840.0 and 1990.0, assuming $\langle \cos \gamma \rangle = 0.65$ and using two possible truncation levels (black line is $L = 8$, red line is $L = 10$). Also presented is the time-dependent rms flow of Amit & Olson (2006) from a full flow inversion of the same historical field model (dashed orange line).

variations of core flow magnitude on decadal timescales that avoids some of the complications associated with full core flow inversions. Excluding the low flow magnitudes prior to 1870, which should probably be interpreted with caution since the field models from this period are based on less comprehensive data, we find here that flow magnitudes varied by 3 km yr^{-1} or ∼25 per cent over several decades.

The main difference between our results and those of Amit & Olson (2006) is that our flow magnitudes are 0–4 km yr^{-1} slower. A possible reason for this discrepancy is that our estimate of the field-flow alignment parameter $\langle \cos \gamma \rangle$ is too large (see Fig. 6). However, the precise rms magnitudes obtained in flow inversions are known to rely heavily on prior assumptions (e.g. choice of damping parameters) not necessarily related to the underlying physics. An example

of this is given in fig. 4(a) of Jackson (1997) where a change of the regularization parameter alters the rms magnitude of the inferred core flow by 5–10 km yr^{-1}, with results particularly sensitive before 1960 when the data constraints are weaker. Similarly, the magnitude of the helical flow inferred by Amit & Olson (2006) and plotted in Fig. 7 depends on an assumed ratio for the horizontal divergence to the radial vorticity of the flow.

Note that the temporal variation of the flow derived from *gufm1* (Fig. 7) is slightly lower (9–12 km yr^{-1}) than our earlier estimate of the core flow magnitude of ∼12.5 km yr^{-1} based on *xCHAOS* (Fig. 6). The reason for this is that the historical field model *gufm1* has lower spatial resolution (especially for SV) than the *xCHAOS* model, with regularization often dominating even below degree 10. The degree to which we can obtain reliable knowledge concerning the core MF and its SV obviously plays an important role in estimates of core flow magnitude. We explore this issue further in the next section.

5.4 Accounting for unresolved small scales

A major uncertainty in applying our method, or any other core flow inversion technique, is that observational knowledge consists only of a spatially low-pass filtered version of the core surface field and its temporal evolution. The origin of this low-pass filter lies in the presence of noise from non-core magnetic sources, in particular crustal magnetization, as well as ionospheric or magnetospheric currents. This problem has been discussed in detail by Hulot *et al.* (1992), and more recently by Eymin & Hulot (2005), Pais & Jault (2008) and Gillet *et al.* (2009), who describe how to account for the interactions of unobserved small-scale field with large-scale flow, and small-scale flow with large-scale field, when inverting large-scale SV to obtain maps of the large-scale flow. Because (10) requires only the MF and SV spectra as inputs, it is possible to systematically study the impact of unobserved small scales on flow magnitude estimates by exploring possible spectral extrapolations; this avenue is not possible for conventional core flow inversions.

Here we explore three possible spectral extrapolations of the MF at the core surface $r = c$. The first was proposed by Roberts *et al.* (2003) as being compatible with the magnetic spectra obtained in numerical dynamo models, while also satisfying the observed large-scale geomagnetic spectrum. It takes the exponential form

$$R_l^R(c) = C_2 e^{-Bl}, \tag{14}$$

with $B = 0.055$. This produces a spectrum similar to that obtained in the high-resolution numerical dynamo model studied by Roberts & Glatzmaier (2000). The constant C_2 is determined, following Lowes (1974) and Roberts *et al.* (2003), by fitting the observed magnetic spectrum for $l \geq 3$ with the dipole and quadrupole terms excluded to obtain a better fit to higher degrees. Hereafter we refer to spectrum (14) as RJC03.

The second spectral extrapolation considered is based on a statistical model of compact eddies motivated by scaling arguments of a magnetostrophic vorticity balance at the core surface (Voorhies *et al.* 2002; Voorhies 2004). As explained by Voorhies (2004), it is the generalization of a spectral form earlier proposed by Stevenson (1983) on the basis of the theory of turbulence expected for a helical dynamo, and it was also suggested by McLeod (1996) from the point of view of a stochastic model of scattered dipole sources at the core surface. It takes the form

$$R_l^V(c) = K \frac{(l + 1/2)}{l(l+1)} \left(\frac{c_s}{c}\right)^{2l+4}, \tag{15}$$

where K is a constant determined by fitting the observed magnetic spectrum. We simplify this model by setting the source radius parameter c_s to the seismologically determined value of the core radius c. Hereafter we refer to spectrum (15) as V04.

The third spectral extrapolation considered is another version of the classic power-law form originally proposed by Lowes (1974). It was recast by Buffett & Christensen (2007) with the purpose of satisfying not only magnetic observations, but also geodetic constrains related to nutations, as well as Ohmic heating requirements. They argued that the following spectral form represents a plausible extrapolation of numerical dynamo model results towards an earth-like regime.

$$R_l^B(c) = \bar{R} \chi^l, \tag{16}$$

where $\bar{R}$ is a constant determined by fitting the non-dipole part of the observed spectrum and $\chi = 0.99$ is fixed to ensure there is sufficient power at short wavelengths to explain nutation observations (for further details see Buffett & Christensen 2007). Although the previous spectral form (14) can be rewritten in the same format as (16), the latter is more restricted as it contains only one free parameter, and forces a very flat spectrum. Note that this extrapolation is less extreme than the completely flat spectral extrapolation recently discussed by Jackson & Livermore (2008). We refer to spectrum (16) as BC07.

To compute $\langle u_H \rangle$ from (10), one requires not only $R_l(c)$ but also the spectra of the SV at the core surface, $Q_l(c)$. We obtain $Q_l(c)$ from $R_l(c)$ by assuming that the ratio between the MF and SV spectra, which physically represents a reorganization time for length scales associated with spherical harmonic degree l (Stacey 1992; Hulot & LeMouël 1994),

$$\tau_l = \sqrt{\frac{R_l(c)}{Q_l(c)}} \tag{17}$$

can be adequately modelled by the power law

$$\tau_l = C_3 l^{-D}, \tag{18}$$

where the constants C_3 and D are determined by an empirical fit to the observed large-scale MF and SV. Holme & Olsen (2006) and Olsen *et al.* (2006) have discussed this empirical law in some detail and have argued that it may reflect the trade-off between advection and diffusion of the magnetic field occurring at all length scales. Substituting (18) into (17) we obtain

$$Q_l(c) = \frac{R_l(c)}{(C_3 l^{-D})^2}. \tag{19}$$

We determined the free parameters in the various spectral extrapolations C_2, K, $\bar{R}$, C_3 and D by least-squares fits to the satellite observation-based *xCHAOS* MF and SV spectra up to degree 10. For the RJC03 spectrum (14), the best fit for $l \geq 3$ was obtained with $C_2 = 1.22 \times 10^{10}$ nT^2, for V04 (15) with $K = 6.97 \times 10^{10}$ nT^2, for the BC07 spectra (16) the best fit to the non-dipole field was obtained with $\bar{R} = 9.20 \times 10^9$ nT^2, while in (18) $C_3 = 778.87$ yr and $D = 1.33$ give the best fit to the ratio of *xCHAOS* MF and SV spectra up to degree $L = 10$. The resulting extrapolations of the MF and SV spectra up to degree $L = 1000$ are presented in Fig. 8.

Using these spectral extrapolations, our preferred value of $\langle \cos \gamma \rangle = 0.65$, and (10), we explored $\langle u_H \rangle$ as a function of the truncation level L. The results of these computations are presented in Fig. 9. We find that for all three spectral extrapolations $\langle u_H \rangle$ increases with L, with equal predicted magnitudes of ∼22 km yr^{-1}
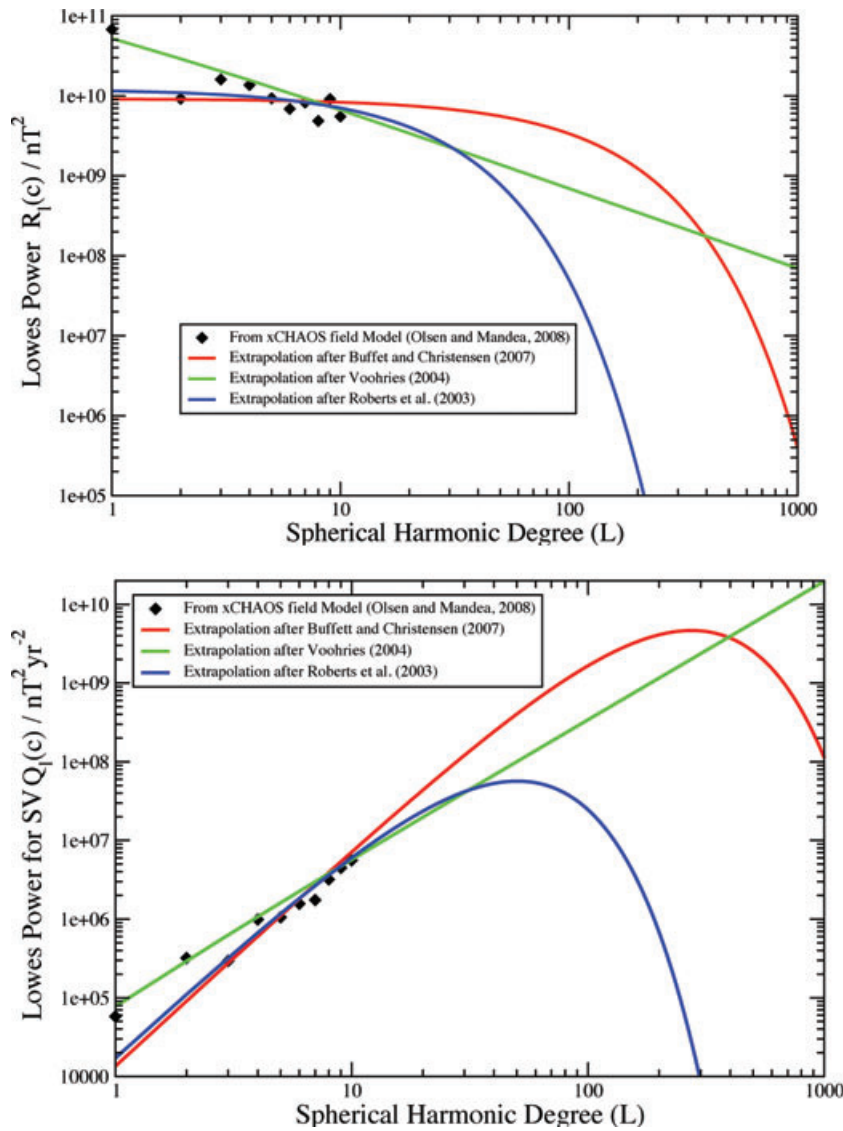
Figure 8. Top panel: Lowes–Mauersberger spatial power spectra of the MF at the core surface from the *xCHAOS* model (Olsen & Mandea 2008) in 2004.0 (black diamonds) and the fit of three possible extrapolations (RJC03: blue line, V04: green line, BC07: red line) extending out to spherical harmonic degree 1000. Bottom panel: Extrapolated spectra for the SV based on (19) and the respective MF spectra.

reached by $L = 40$. The predictions of the different extrapolations begin to differ markedly above $L = 60$. For $L > 150$ the prediction of RJC03 reaches an asymptotic value of 29 km yr^{-1}. The extrapolations V04 and BC07 are practically identical until $L = 200$, where $\langle u_H \rangle \sim 41$ km yr^{-1}. For larger L the predictions of BC07 and V04 diverge, with V04 growing exponentially, while BC07 reaches an asymptotic value of ~ 56 km yr^{-1} for $L > 1000$.

Fig. 10 summarizes a large number of calculations focusing on the BC07 extrapolation and exploring a very wide range of values for both $\langle \cos \gamma \rangle$ and the truncation degree L. It should however be remembered that Buffett & Christensen (2007) argued their spectrum is capable of satisfying geodetic constraints derived from nutation observations, while remaining compatible with Ohmic heating constraints, only for a truncation degree in the range $160 < L < 250$. More generally, Fig. 10 shows that to obtain flow speeds in excess of 60 km yr^{-1}, with the BC07 spectral extrapolation, it is necessary for $\langle \cos \gamma \rangle$ to be less than 0.6. Flow speeds are always less than

50 km yr^{-1} if $\langle \cos \gamma \rangle$ lies between 0.4 and 0.8 and the truncation degree is less than 100.

What truncation degree L, above which magnetic dissipation dominates and the magnetic spectrum decays, is appropriate for the Earth's core? Unfortunately the Ohmic dissipation scale in the Earth's core is not known. Christensen & Tilgner (2004), in a study of scaling laws in numerical and experimental dynamos, concluded that a magnetic dissipation time of 42 yr was appropriate for the Earth's core. This corresponds to a length scale of $\mathcal{L}_{diss} \sim 50$ km (see also Buffett & Christensen 2007) or a spherical harmonic degree $L = \pi D / \mathcal{L}_{diss} \sim 150$. Beyond this dissipation scale, magnetic diffusion is expected to dominate SV, the frozen-flux approximation fails and our method would become inapplicable. As can be seen from Fig. 9, taking $L = 150$ leads to predictions of $\langle u_H \rangle \sim 29$ km yr^{-1} from the RJC03 extrapolation, 38 km yr^{-1} from the BC07 extrapolation and 37 km yr^{-1} from the V04 extrapolation, all with $\langle \cos \gamma \rangle = 0.65$. For upper estimates obtained using $\langle \cos \gamma \rangle = 0.60$ and $L = 250$ (equivalent to a dissipation
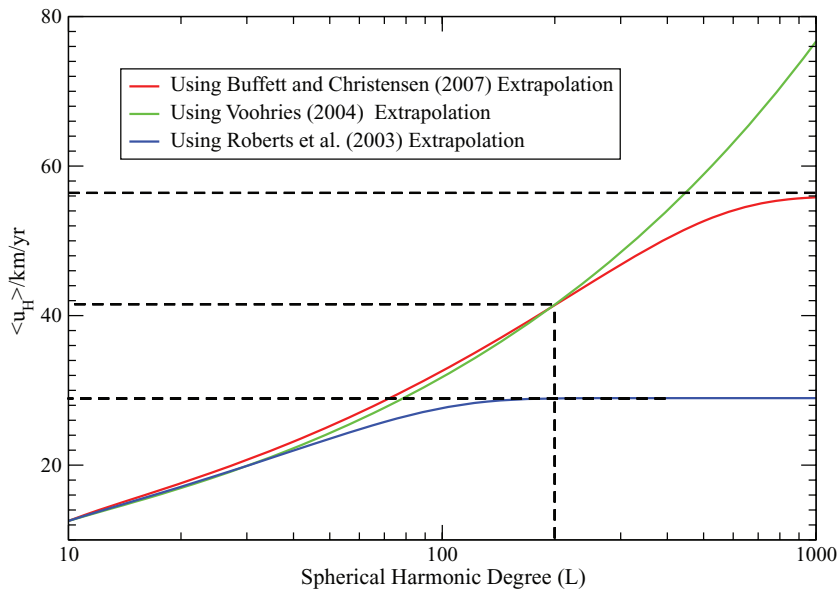
Figure 9. Estimates of the core flow magnitude $\langle u_H \rangle$ as a function of spherical harmonic degree of truncation L of the MF and SV for the spectral extrapolations of BC07 (red), V04 (green) and RJC03 (blue).
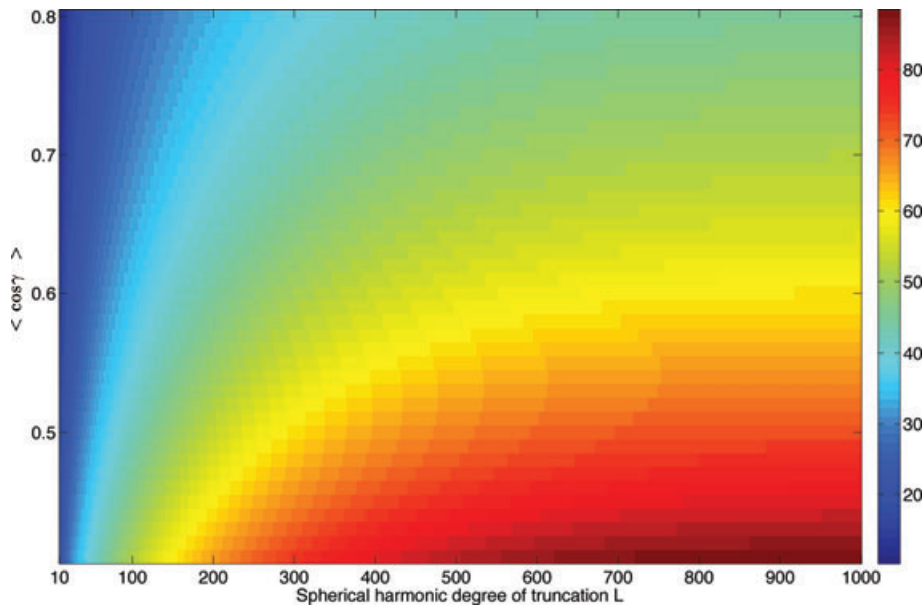
Figure 10. Colour scale plot of the predicted flow magnitude $\langle u_H \rangle$ in km yr^{-1} at the core surface, accounting for the effect of unobserved small scales, derived from (10) for a wide range of $\langle \cos \gamma \rangle$ between 0.4 and 0.8 and using the observed spectra from *xCHAOS* in 2004.0 (to degree $L = 10$) extrapolated up to $L = 1000$ using BC07 form (16) and the assumption that (19) holds for the SV spectrum.

scale $\sim$30 km), RJC03 predicts a flow magnitude of 31 km yr^{-1}, BCO7 predicts 48 km yr^{-1} while V04 predicts a similar amplitude of 49 km yr^{-1}. Rounding to 50 km yr^{-1} gives what we take to be an upper estimate for the plausible magnitude of flow at the Earth's core surface, accounting for the influence of unobserved small scales. Note that for almost flat MF spectra such as BC07 and V04 having L much larger than 250 will produce more Ohmic heating than is thought to be reasonable. Readers should bear in mind that our upper estimate of 50 km yr^{-1} depends both on the spectral extrapolations employed and on the assumed magnetic dissipation scale for the Earth's core, so it is not a formal upper bound.

6 DISCUSSION

The intermediate value of $\langle \cos \gamma \rangle = 0.6$–0.7 suggested by scaling law (13) for the Earth's core, indicates a combined influence of regions of field-aligned flow near high-latitude intense flux patches [as also seen in numerical dynamos with tomographic outer boundary heat flux (Amit *et al.* 2010)] and mid- to low-latitude regions where flow is more often perpendicular to B_r-contours. This degree of field-flow alignment is compatible with earlier helical core flow inversions which reported a ratio of 1.2–1.4 between the flow parallel and the flow perpendicular to B_r-contours, corresponding to $\langle \cos \gamma \rangle \sim 0.58$–0.64 (Amit & Olson 2004; Amit & Olson 2006).

Table 4. Estimates of non-dimensional parameters for the Earth's core. The flow magnitude is calculated with and without spectral extrapolation, for two choices of field-flow alignment factor (for $\langle \cos \gamma \rangle = 0.6$ and 0.7), and for various choices of field and flow length scales. In the extrapolated cases, the flow length scale is taken to be that of the maximum in the SV spectrum so that $\mathcal{L}_u = \pi D/L_{SVmax}$, unless this is below the dissipation length scale defined by the truncation degree $\mathcal{L}_{diss} = \pi D/L$, in which case $\mathcal{L}_u = \mathcal{L}_{diss}$. Here D is the shell thickness which is 2260 km for the Earth's core. Three choices for $\mathcal{L}_B$ are considered. These are $\mathcal{L}_B^h$ (1000 km as associated with the large-scale observed magnetic field), $\mathcal{L}_B^{h'}$ (the same as $\mathcal{L}_u$) and $\mathcal{L}_B^r$ (based on a radial length scale of 40 km for the magnetic diffusive boundary layer). All results are reported to two significant figures. A magnetic diffusivity for the Earth's core of 1 m² s⁻¹ and a rotation rate of $\Omega = 7.3 \times 10^{-5}$ s⁻¹ have been used. Conventional estimates for Ro and Rm using $\mathcal{L}_B^h$ are highlighted in bold.

Extrap.	Sph. harm. Trunc. Deg L	$\mathcal{L}_{diss}$ (km)	$\langle \cos \gamma \rangle$	$\langle \boldsymbol{u_H} \rangle$ (km yr⁻¹)	$\mathcal{L}_u$ (km)	$\mathcal{L}_B^h$ (km)	$\mathcal{L}_B^{h'}$ (km)	$\mathcal{L}_B^r$ (km)	Ro $\dfrac{\langle \boldsymbol{u_H} \rangle}{\Omega \mathcal{L}_u}$	Rm $\dfrac{\langle \boldsymbol{u_H} \rangle \mathcal{L}_B^h}{\eta}$	Rm' $\dfrac{\langle \boldsymbol{u_H} \rangle \mathcal{L}_B^{h'}}{\eta}$	Rm$_r$ $\dfrac{\langle \boldsymbol{u_H} \rangle (\mathcal{L}_B^r)^2}{\eta \mathcal{L}_B^h}$	Rm'$_r$ $= \dfrac{\langle \boldsymbol{u_H} \rangle (\mathcal{L}_B^r)^2}{\eta \mathcal{L}_B^{h'}}$
None	10	1000	0.7	11	1000	1000		40	**4.9 × 10⁻⁶**	**350**		0.55	
None	10	1000	0.6	14	1000	1000		40	**6.1 × 10⁻⁶**	**440**		0.71	
RJC03	150	48	0.7	27	160	1000	160	40	7.3 × 10⁻⁵	860	140	1.4	8.6
RJC03	150	48	0.6	31	160	1000	160	40	8.4 × 10⁻⁵	980	160	1.6	9.8
RJC03	250	28	0.7	27	160	1000	160	40	7.3 × 10⁻⁵	860	140	1.4	8.6
RJC03	250	28	0.6	31	160	1000	160	40	8.4 × 10⁻⁵	980	160	1.6	9.8
BC07	150	48	0.7	35	48	1000	48	40	3.2 × 10⁻⁴	1100	53	1.8	37
BC07	150	48	0.6	41	48	1000	48	40	3.7 × 10⁻⁴	1300	62	2.1	43
BC07	250	28	0.7	41	30	1000	30	40	5.9 × 10⁻⁴	1300	39	2.1	69
BC07	250	28	0.6	48	30	1000	30	40	4.9 × 10⁻⁴	1500	46	2.4	81
V04	150	48	0.7	35	48	1000	55	40	3.2 × 10⁻⁴	1100	53	1.8	37
V04	150	48	0.6	40	48	1000	55	40	3.6 × 10⁻⁴	1300	61	2.0	42
V04	250	28	0.7	42	28	1000	30	40	6.5 × 10⁻⁴	1300	37	2.1	71
V04	250	28	0.6	49	28	1000	30	40	7.6 × 10⁻⁴	1600	44	2.5	89

The estimate of $\langle \boldsymbol{u_H} \rangle = 11$–14 km yr⁻¹, derived from (10) using the *xCHAOS* MF and SV without any spectral extrapolation, using the range $\langle \cos \gamma \rangle = 0.6$–0.7 inferred from numerical dynamo models, also lies well within the range of flow magnitudes reported in previous studies (see Table 1). Temporal variations in flow magnitude inferred from investigations with the MF and SV from *gufm1* were further found to be in qualitative agreement with fluctuations previously inferred in full flow inversions of SV (Jackson 1997; Amit & Olson 2006), and with geodetic inferences of changes in the length of day. These agreements give confidence that the approach presented here is sensible, encouraging us to explore its implications when extrapolated to unobserved length scales.

We have demonstrated that $\langle \boldsymbol{u_H} \rangle$ could conceivably be as large as 50 km yr⁻¹, depending on details of the unobserved MF and SV spectra, and on the length scale at which dissipation forces the magnetic spectrum to decay. This upper estimate is notably higher than previous estimates of the core flow magnitude (see Table 1). The source of the discrepancy is that we have explicitly quantified the influence of unobserved small scales which were inaccessible in previous studies. On the other hand, for $\langle \boldsymbol{u_H} \rangle$ to be larger than 50 km yr⁻¹, either $\langle \cos \gamma \rangle$ must be less than 0.6 (unlikely according to the dynamos we have studied), the magnetic spectra must be flatter and contain more power at small scales than either the BC07 or V04 spectra (though these spectra are already very flat compared to most existing numerical dynamos), or the magnetic dissipation scale in the Earth's core must be considerably less than the minimum length scale of 30 km that we have considered (probably unlikely from Ohmic heating considerations, see Buffett & Christensen 2007; Christensen 2010). We therefore propose that 50 km yr⁻¹ is a defensible, if rather extreme, upper estimate of how strong flow in the Earth's core could possibly be.

It should however be emphasized that 50 km yr⁻¹ is in our opinion a rather extreme upper estimate of the magnitude of the core surface flow. The actual value of $\langle \boldsymbol{u_H} \rangle$ could be considerably less than 50 km yr⁻¹, and may in fact lie closer to our initial estimate of

$\langle \boldsymbol{u_H} \rangle \sim 11$–14 km yr⁻¹ derived from the observed MF and SV without any extrapolation. The latter scenario would require that the magnetic energy spectrum in the Earth's core decays much more rapidly than in BC07 model and that there is an alternative coupling mechanism to enable the geodetic constraints to be satisfied (see, e.g. Deleplace & Cardin 2006). It is noteworthy that in many low Pm MHD systems the magnetic energy spectrum has its dissipation scale at larger length scales (at smaller L) than the kinetic energy spectrum (Ponty *et al.* 2004; Schaeffer & Cardin 2006; Takahashi *et al.* 2008; Brandenberg 2009).

We now use our estimates of $\langle \boldsymbol{u_H} \rangle$ to compute the non-dimensional parameters Rm, Rm$_r$ and Ro that give valuable insight into the dynamic and kinematic regimes in the Earth's core. In Table 4 we explore a range of estimates of these parameters based on conceivable values for $\langle \cos \gamma \rangle$ and possible length scales of the field and flow at the core surface. Precise definitions of the parameters and details concerning the choices of length scales are provided in the table caption.

With $\langle \boldsymbol{u_H} \rangle = 11$–14 km yr⁻¹ and taking $\mathcal{L}_u = \mathcal{L}_B^h = 1000$ km we obtain conventional estimates of Rm $\sim$ 350–440 and Ro $\sim$ 5–6 × 10⁻⁶ in agreement with previous studies. By considering the range of alternative estimates for these non-dimensional numbers presented in Table 4 one can, however, see that the assumptions made concerning the unobserved small scales of the field and flow are critical; nonetheless some general conclusions may be drawn.

A first conclusion is that given the range of $\langle \cos \gamma \rangle \sim 0.6$–0.7, and exploring the three possible extrapolations of the MF and SV with two choices of truncation degree, the magnitude of the core surface flow $\langle \boldsymbol{u_H} \rangle$ is found to lie in the range 27–50 km yr⁻¹. Note that for a wider range of $\langle \cos \gamma \rangle$, the range of flow magnitudes is simply linearly stretched. For example, with $\langle \cos \gamma \rangle = 0.55$–0.75 a revised flow magnitude range of $\langle \boldsymbol{u_H} \rangle = 25$–55 km yr⁻¹ is obtained.

Using our favoured range of 27–50 km yr⁻¹, if a length scale of 1000 km is adopted for the horizontal magnetic field, then Rm lies in the range 350–1600. Instead assuming that the horizontal length

scale of the magnetic field is the same as that of the velocity field (thus taking into account smaller scales), we find Rm′ is considerably smaller, in the range 37–160. Assuming a radial length scale of 40 km associated with the magnetic diffusion boundary layer [the estimate of Chulliat & Olsen (2010) with $\eta = 1\,\mathrm{m^2\,s^{-1}}$], and adopting a large horizontal length scale of 1000 km, then Rm_r is found to lie in the range 0.5–2.5. This indicates that radial magnetic diffusion could become comparable to magnetic advection in some locations. Accounting for both radial magnetic diffusion and assuming a small horizontal length scale for the magnetic field gives Rm'_r of 8–90 suggesting that magnetic advection generally dominates, though diffusive effects may be more important than is commonly assumed. This scenario agrees with inferences from a study of numerical dynamos (Amit & Christensen 2008) and with the conclusions of some studies of observed geomagnetic field evolution (Bloxham & Gubbins 1986; Chulliat & Olsen 2010).

Regarding the Rossby number, we find $5 \times 10^{-6} < \mathrm{Ro} < 8 \times 10^{-4}$, that is, inertia is always very small compared to the Coriolis force, even when the influence of small-scale flows is considered. For comparison, the historical time-variations in the flow magnitude inferred in Section 5.3 permit an order of magnitude estimate of the flow accelerations $|\partial \boldsymbol{u}/\partial t|$ compared to the Coriolis acceleration $|\Omega \times \boldsymbol{u}|$. Changes in the core flow magnitude of 25 per cent over an interval of 40 yr as found in Fig. 7 lead to an estimate of $\mathrm{Ro} \sim |\partial \boldsymbol{u}/\partial t|/|\Omega \times \boldsymbol{u}| \sim 1 \times 10^{-5}$. This agrees well with the estimate of 2×10^{-5} previously obtained by Olsen & Mandea (2008) who derived core flow maps from satellite geomagnetic observations. It is noteworthy that even if one adopts our largest estimate of the Rossby number, the effects of inertia are still more than factor 100 smaller than the critical (local) Rossby number that is proposed as the transition point between non-reversing to reversing dynamos (Olson & Christensen 2006; Christensen 2010).

When evaluating the above results one should remember that our flow magnitude estimation scheme involves a number of assumptions, and has some fundamental limitations. First, it was assumed from the outset that frozen-flux is a good approximation on average, and that toroidal flows dominate at the core surface. Secondly, the inferred values for $\langle \cos \gamma \rangle$ were derived from a limited suite of numerical dynamo models whose control parameters were restricted by the available computing power. Thirdly, the form and truncation level of the spectral extrapolations of the MF and SV remain uncertain; we have simply explored some possible scenarios. Fourthly, the methodology is restricted to the study of flow at the surface of the core and cannot probe the flow within the volume of the outer core, unless further assumptions are made. Ideally estimates of the flow within the volume would enter into Ro and Rm. For the suite of numerical dynamo models we have studied, the ratio between the magnitude of the flow at the core surface and that averaged over the volume of the outer core takes values between 1.16 and 1.27 with no obvious dependence on control parameters (see also Christensen & Aubert 2006), so it is unclear how to accurately infer volumetric flow magnitude from surface flow. Finally, there remains some uncertainty in the exact value of the magnetic diffusivity with published values ranging between 1 and 3 $\mathrm{m^2 s^{-1}}$ (Secco & Schloessin 1989; Poirier 2000; Stacey & Loper 2007). Despite these limitations, the scheme we have presented performed well in synthetic tests, is consistent with the large-scale estimates of previous studies, and enables one to quantify the effects of small-scale field and flow on core flow magnitude estimates. The inferred values of Ro and Rm for the Earth's core therefore provide useful guidance concerning the dynamic and kinematic regimes of the geodynamo.

7 CONCLUDING REMARKS

A new approach for estimating the rms flow magnitude $\langle \boldsymbol{u}_H \rangle$ at Earth's core surface has been presented and validated using numerical dynamo models. The method is capable of accounting for both field-aligned flow and unobserved small scales. We estimate that $\langle \boldsymbol{u}_H \rangle$ lies within the range 11–50 km yr^{-1}. The lower estimate of 11 km yr^{-1} comes from considering only the part of the flow that can be constrained by geomagnetic observations (i.e. it involves no spectral extrapolation) and it is in agreement with previous estimates. The upper estimate of 50 km yr^{-1} is not a hard bound, but is an extreme scenario consistent with the observed geomagnetic spectrum and with presently available numerical dynamo models. Study of field-flow alignment in numerical dynamos has revealed that in the vicinity of high-latitude convective rolls the field and the flow are well aligned resulting in low induction efficiency there. At lower latitudes zonal flow can often be perpendicular to contours of B_r, leading to efficient induction and enhanced SV in these regions.

Applications of the method presented here need not be restricted to Earth's core. Similar schemes could be applied to any MHD system with sufficiently high Rm, so that the majority of the field evolution occurs by a frozen-flux induction mechanism, and where toroidal flow dominates close to the outer boundary. To obtain the required prior knowledge concerning $\langle \cos \gamma \rangle$, sufficient numerical dynamo model runs with appropriate geometry, kinematics and (as far as possible) force balance, do however need to be carried out. Finally sufficient high-quality observations of the magnetic field and its temporal variability must be available to determine the MF and SV spectra.

One possible future application could be to monitor the magnitude of flow in the cores of other planetary bodies. For example, terrestrial planets or solid-ice satellites generating planetary scale magnetic fields (such as Mercury or Ganymede) could be feasible subjects. The method could also perhaps be applied to rotating MHD experiments carried out in a spherical geometry to study dynamo action or magnetostrophic dynamics (Cardin & Brito 2007), if these are monitored using magnetic observations. It is very difficult to directly observe fluid motions in liquid metals by visual means, due to their opacity, and doppler ultrasonic measurements are challenging and give only local estimates (Brito *et al.* 2001). A possible obstacle may be the requirement that field evolution occurs primarily by frozen-flux advection; existing experiments typically have Rm not much greater than 1, so it is unclear whether the frozen-flux hypothesis is a reasonable approximation even on short timescales. It would however be of great interest to test the method directly using a controlled natural system, rather than relying on synthetic tests with numerical dynamo models.

According to our new upper estimate for the flow magnitude in the Earth's core of 50 km yr^{-1}, it is no longer reasonable to argue that unquantified field-aligned and small-scale flows permit flow magnitudes many orders of magnitudes larger than the traditional estimates of 10–20 km yr^{-1}. To obtain more refined estimates, a better understanding of the factors controlling the unobserved part of the MF and SV spectra is required. Further study of field-flow alignment in numerical dynamo models spanning a wider range of control parameters, including investigation of regions within the volume where dynamo action takes place, may also provide fresh insight to the nature of the geodynamo process.

REFERENCES

Amit, H. & Christensen, U.R., 2008. Accounting for magnetic diffusion in core flow inversions from geomagnetic secular variation, *Geophys. J. Int.,* **175**, 913–924.

Amit, H. & Olson, P., 2004. Helical core flow from geomagnetic secular variation, *Phys. Earth planet. Inter.,* **147**, 1–25.

Amit, H. & Olson, P., 2006. Time-average and time-dependent parts of core flow, *Phys. Earth planet. Inter.,* **155**, 120–139.

Amit, H., Olson, P. & Christensen, U.R., 2007. Tests of core flow imaging methods with numerical dynamos, *Geophys. J. Int.,* **168**, 27–39.

Amit, H., Aubert, J. & Hulot, G., 2010. Stationary, oscillating or drifting mantle-driven flux patches, *J. geophys. Res.,* **115**, doi:10.1029/2009JB006542.

Archontis, V., Dorch, S.B.F. & Nordlund, A., 2007. Nonlinear MHD dynamo operating at equipartition, *Astron. Astrophys.,* **472**, 715–726.

Backus, G., 1968. Kinematics of geomagnetic secular variation in a perfectly conducting core, *Phil. Trans. R. Soc. Lond. A.,* **263**, 239–266.

Backus, G. & LeMouël, J.L., 1986. The region on the core mantle boundary where a geostrophic velocity field can be determined from frozen flux magnetic data, *Geophys. J. R. astr. Soc.,* **85**, 617–628.

Backus, G., Parker, R.L. & Constable, C.G., 1996. *Foundations of Geomagnetism,* pp. 247–260, Cambridge Univ. Press, Cambridge.

Beggan, C. & Whaler, K., 2008. Core flow modelling assumptions, *Phys. Earth planet. Inter.,* **167**, 217–222.

Bloxham, J., 1989. Simple models of fluid flow at the core surface derived from geomagentic field models, *Geophys. J. Int.,* **99**, 173–182.

Bloxham, J., 1992. The steady part of the secular variation of the Earth's magnetic field, *J. geophys. Res.,* **97**, 19 565–19 579.

Bloxham, J. & Gubbins, D., 1986. Geomagnetic field analysis, IV. Testing the frozen-flux hypothesis, *Geophys. J. Int.,* **84**, 139–152.

Bloxham, J. & Jackson, A., 1989. Simultaneous stochastic inversion for geomagnetic main field and secular variation, II: 1820-1980, *J. geophys. Res.,* **94**, 15 753–15 769.

Bloxham, J. & Jackson, A., 1991. Fluid flow near the surface of the Earth's outer core, *Rev. Geophys.,* **29**, 97–120.

Booker, J.R., 1969. Geomagnetic data and core motions, *Proc. R. Soc. Lond. A.,* **309**, 27–40.

Brandenberg, A., 2009. Large scale dynamos at low magnetic Prandtl numbers, *Astrophys. J.,* **697**, 1206–1213.

Brito, D., Nataf, H., Cardin, P., Aubert, J. & Masson, J.P., 2001. Ultrasonic doppler velocimetry in liquid gallium, *Exp. Fluids,* **31**, 653–663.

Buffett, B.A. & Christensen, U.R., 2007. Magnetic and viscous coupling at the core-mantle boundary: inferences from observations of the Earth's nutations, *Geophys. J. Int.,* **171**, 145–157.

Bullard, E.C. & Gellman, H., 1950. Homogeneous dynamos and terrestrial magnetism, *Phil. Trans. R. Soc. Lond. A.,* **247**, 213–278.

Bullard, E.C., Freedman, C., Gellman, H. & Nixon, J., 1950. The westward drift of the Earth's magnetic field, *Phil. Trans. R. Soc. Lond. A.,* **243**, 67–92.

Cameron, R. & Galloway, D., 2006. Saturation properties of the Archontis dynamo, *Mon. Not. R. astr. Soc.,* **365**, 735–746.

Cardin, P. & Brito, D., 2007. Survey of experimental results, in *Mathematical Aspects of Natural Dynamos,* pp. 361–407, eds Dormy, E. & Soward, A.M., CRC Press, Boca Raton, FL.

Cattaneo, F. & Tobias, S.M., 2009. Dynamo properties of the turbulent velocity field of a saturated dynamo, *J. Fluid. Mech.,* **621**, 205–214.

Christensen, U.R., 2010. Dynamo scaling laws and applications to the planets, *Space Sci. Rev.,* **152**, 565–590.

Christensen, U.R. & Aubert, J., 2006. Scaling properties of convection-driven dynamos in rotating spherical shells and applications to planetary magnetic fields, *Geophys. J. Int.,* **166**, 97–114.

Christensen, U.R. & Tilgner, A., 2004. Power requirement of the geodynamo from ohmic losses in numerical and laboratory dynamos, *Nature,* **439**, 169–171.

Christensen, U.R. et al., 2001. A numerical dynamo benchmark, *Phys. Earth. planet. Int.,* **128**, 25–34.

Chulliat, A. & Olsen, N., 2010. Observation of magnetic diffusion in the Earth's outer core from Magsat, Ørsted, and CHAMP data, *J. geophys. Res.,* **115**, B05105, doi:10.1029/2009JB006994.

Deleplace, B. & Cardin, P., 2006. Viscomagnetic torque at the core mantle boundary, *Geophys. J. Int.,* **167**, 557–566.

Elsasser, W.M., 1939. On the origin of the Earth's magnetic field, *Phys. Rev,* **55**, 489–498.

Elsasser, W.M., 1946. Induction effects in terrestrial magnetism. Part II. The secular variation, *Phys. Rev,* **70**, 202–212.

Elsasser, W.M., 1950a. The Earth's interior and geomagnetism, *Rev. Mod. Phys.,* **22**, 1–40.

Elsasser, W.M., 1950b. The hydromagnetic equations, *Phys. Rev,* **79**, 183–183.

Eymin, C. & Hulot, G., 2005. On surface core flows inferred from satellite magnetic data, *Phys. Earth planet. Inter.,* **152**, 200–220.

Finlay, C.C., Dumberry, M., Chulliat, A. & Pais, M., 2010. Short timescale core dynamics: theory and observationns, *Space Sci. Rev.,* **155**, 177–218.

Gillet, N., Pais, M.A. & Jault, D., 2009. Ensemble inversion of time-dependent core flow models., *Geochem. Geophys. Geosyst.,* **10**, Q06004, doi:10.1029/2008GC002290.

Gillet, N., Lesur, V. & Olsen, N., 2010. Ensemble inversion of time-dependent core flow models., *Space Sci. Rev.,* **155**, 129–145.

Gire, C. & LeMouël, J.L., 1990. Tangentially geostrophic flow at the core-mantle boundary compatible with the observed geomagnetic secular variation: the large-scale component of the flow, *Phys. Earth planet. Inter.,* **59**, 259–287.

Gubbins, D., Barber, C.N., Gibbons, S. & Love, J.J., 2000. Kinematic dynamo action in a sphere: I effects of differential rotation and meridional circulation on solutions with axial dipole symmetry, *Proc. R. Soc. Lond.,* **A456**, 1333–1353.

Holme, R., 2007. Large-scale flow in the core, in *Treatise on Geophysics,* Vol. 8, pp. 107–130, ed. Olson, P., Elsevier Science, Amsterdam.

Holme, R. & Olsen, N., 2006. Core surface flow modelling from high-resolution secular variation, *Geophys. J. Int.,* **166**, 518–528.

Hulot, G. & LeMouël, J.L., 1994. A statistical approach to the Earth's main magnetic field, *Phys. Earth planet. Inter.,* **82**, 167–183.

Hulot, G., LeMouël, J.L. & Wahr, J., 1992. Taking into account truncation problems and geomagnetic model accuracy in assessing computed flows at the core-mantle boundary, *Geophys. J. Int.,* **108**, 224–246.

Jackson, A., 1997. Time-dependency of tangentially geostrophic core surface motions, *Phys. Earth planet. Inter.,* **103**, 293–311.

Jackson, A. & Finlay, C.C., 2007. Geomagnetic secular variation and its applications to the core, in *Treatise on Geophysics,* Vol. 5, pp. 147–193, ed. Olson, P., Elsevier Science, Amsterdam.

Jackson, A. & Livermore, P.W., 2008. On Ohmic heating in the Earth's core I: nutation constraints, *Geophys. J. Int.,* **177**, 367–382.

Jackson, A., Bloxham, J. & Gubbins, D., 1993. Time-dependent flow at the core surface and conservation of angular momentum in the coupled core-mantle system, in *Dynamics of Earth's Deep Interior and Earth Rotation,* eds LeMouël, J.-L., Smylie, D. & Herring, T., *AGU/IUGG.*

Jackson, A., Jonkers, A.R.T. & Walker, M.R., 2000. Four centuries of geomagnetic secular variation from historical records, *Phil. Trans. R. Soc. Lond.,* **A358**, 957–990.

Kahle, A., Ball, R.H. & Vestine, E.H., 1967a. Comparison of estimated surface fluid motions of the core for various epochs, *J. geophys. Res.,* **72**, 1095–1108.

Kahle, A., Vestine, E.H. & Ball, R., 1967b. Estimated surface motions of the Earth's core, *J. geophys. Res.,* **72**, 4917–4925.

Kutzner, C. & Christensen, U.R., 2002. From stable dipolar towards reversing numerical dynamos, *Phys. Earth. planet. Inter.,* **131**, 29–45.

Langlais, B., Mandea, M. & Ultre-Guerard, P., 2003. High resolution magnetic field modelling: application to MAGSAT and Ørsted data, *Phys. Earth. planet. Inter.,* **135**, 77–91.

LeMouël, J.L., 1984. Outer core geostrophic flow and secular variation of Earth's magnetic field, *Nature,* **311**, 734–735.

Lesur, V., Wardinski, I., Rother, M. & Mandea, M., 2008. GRIMM: the GFZ reference internal magnetic model based on vector satellite and observatory data, *Geophys. J. Int.,* **173**, 382–394.

Lesur, V., Wardinski, I., Asari, S., Minchev, B. & Mandea, M., 2010. Modelling the Earth's core magnetic field under flow constraints, *Earth, Planets Space,* **10**, 503–516.

Lloyd, D. & Gubbins, D., 1990. Toroidal fluid motion at the top of Earth's core, *Geophys. J. Int.,* **100**, 455–467.

Lowes, F.J., 1966. Mean-square values on the sphere of spherical harmonic vector fields, *J. geophys. Res.,* **71**, 2179.

Lowes, F.J., 1974. Spatial power spectrum of the main geomagnetic field, *Geophys. J. R. astr. Soc.,* **36**, 717–730.

Mason, J., Cattaneo, F. & Boldyrev, S., 2006. Dynamic alignment in driven magnetohydrodynamic turbulence, *Phys. Rev. Lett.,* **97**, 255002, doi:10.1103/PhysRevLett.97.25502.

Mauersberger, P., 1956. Das mittel der energiedichte des geomagnetischen hauptfeldes and der erderflaeche unde seine saekulare anderung, *Anderung, Gerlands Beitr. Geophys.,* **65**, 207–215.

McLeod, M.G., 1996. Spatial and temporal power spectra of the geomagnetic field, *J. geophys. Res,* **101**, B2, 2745–2763.

Moffatt, H.K., 1978. *Magnetic Field Generation in Electrically Conducting Fluids,* Cambridge Univeristy Press, Cambridge.

Nagata, T. & Syono, Y., 1961. Geomagnetic secular variation during the period from 1955 to 1960, *J. Geomagnet. Geoelec.,* **12**, 84–98.

Olsen, N. & Mandea, M., 2008. Rapidly changing flows in the Earth's core, *Nat. Geosci.,* **1**, 390–394.

Olsen, N., Lühr, H., Sabaka, T.J., Mandea, M., Rother, M., Tøffner-Clausen, L. & Choi, S., 2006. CHAOS: a model of the Earth's magnetic field derived from CHAMP, Ørsted and SAC-C magnetic satellite data, *Geophys. J. Int.,* **166**, 67–75.

Olson, P. & Christensen, U.R., 2002. The time averaged magnetic field in numerical dynamos with nonuniform boundary heat flow, *Geophys. J. Int.,* **151**, 809–823.

Olson, P. & Christensen, U.R., 2006. Dipole moment scaling for convection-driven planetary dynamos, *Earth planet. Sci. Lett.,* **250**, 561–571.

Olson, P., Christensen, U.R. & Glatzmaier, G.A., 1999. Numerical modeling of the geodynamo: mechanisms of field generation and equilibration, *J. geophys. Res.,* **104**, 10 383–10 404.

Olson, P., Sumita, I. & Aurnou, J., 2002. Diffusive magnetic images of core upwellings, *J. geophys. Res.,* **107**, doi:10.1029/JB000384.

Pais, M.A. & Jault, D., 2008. Quasi-geostrophic flows responsible for the secular variation of the Earth's magnetic field, *Geophys. J. Int.,* **173**, 421–443.

Pais, M.A., Oliveira, O. & Nogueira, F., 2004. Nonuniqueness of inverted core-mantle boundary flows and deviations from tangential geostrophy, *J. geophys. Res.,* **109**, B08105, doi:10.1029/2004JB003012.

Perez, J.C. & Boldyrev, S., 2007. Role of cross-helicity in magnetohydrodynamic turbulence, *Phys. Rev. Lett.,* **102**, 025003, doi:10.1103/PhysRevLett.102.025003.

Poirier, J.P., 2000. *Introduction to the Physics of the Earth's Interior,* Cambridge University Press, Cambridge.

Ponty, Y., Politano, H. & Pinton, J.F., 2004. Simulation of induction at low magnetic Prandtl number, *Phys. Rev. Lett.,* **92**, 1144503, doi:10.1103/PhysRevLett.92.144503.

Rau, S., Christensen, U.R., Jackson, A. & Wicht, J., 2000. Core flow inversion tested with numerical dynamo models, *Geophys. J. Int.,* **141**, 485–497.

Roberts, P.H. & Glatzmaier, G.A., 2000. A test of the frozen flux approximation using a new geodynamo model, *Phil. Trans. R. Soc. Lond. A.,* **358**, 1109–1121.

Roberts, P.H. & Scott, S., 1965. On analysis of the secular variation, 1, a hydromagnetic constraint: theory, *J. Geomagn. Geoelectr.,* **17**, 137–151.

Roberts, P.H., Jones, C.A. & Calderwood, A.R., 2003. Energy fluxes and ohmic dissipation in the Earth's core, in *Earth's Core and Lower Mantle,* eds Jones, C., Soward, A. & Zhang, K., Taylor and Francis, London.

Schaeffer, N. & Cardin, P., 2006. Quasi-geostrophic kinematic dynamos at low magnetic Prandtl number, *Earth planet. Sci. Lett.,* **245**, 595–604.

Schrinner, M., Schmitt, D., Cameron, R. & Hoyng, P., 2010. Saturation and time dependence of geodynamo models, *Geophys. J. Int.,* **182**, 675–681.

Secco, R.A. & Schloessin, H.H., 1989. The electrical resistivity of solid and Fe at pressures up to 7 GPa, *J. geophys. Res.,* **94**, 5887–5894.

Sreenivasan, B. & Jones, C.A., 2006. The role of inertia in the evolution of spherical dynamos, *Geophys. J. Int.,* **164**, 467–476.

Stacey, F.D., 1992. *Physics of the Earth,* Brookfield Press, Brisbane.

Stacey, F.D. & Loper, D.E., 2007. A revised estimate of the conductivity of iron alloy at high pressure and implications for the core energy balance, *Phys. Earth planet. Int.,* **161**, 13–18.

Stevenson, D.J., 1983. Planetary magnetic fields, *Rep. Prog. Phys.,* **46**, 555–620.

Takahashi, F. & Matsushima, M., 2005. Dynamo action in a rotating spherical shell at high Rayleigh numbers, *Phys. Fluids,* **17**, 076601, doi:10.1063/1.1972016.

Takahashi, F., Matsushima, M. & Honkura, Y., 2008. Scale variability in convection-driven MHD dynamos at low Ekman number, *Phys. Earth planet. Inter.,* **167**, 168–178.

Vestine, E.H., Laporte, L., Cooper, C., Lange, I. & Hendrix, W.C., 1947. *Description of the Earth's Main Magnetic Field and its Secular Change,* Carnegie Institution Publ., Washington, DC.

Voorhies, C.V., 1986. Steady flows at the top of Earth's core derived from geomagnetic field models, *J. geophys. Res.,* **91**, 12 444–12 466.

Voohries, C.V., 2004. Narrow-scale flow and a weak field by the top of Earth's core: evidence from Ørsted, magsat and secular variation, *J. geophys. Res.,* **109**, B03106, doi:10.1029/2003JB002833.

Voohries, C.V., Sabaka, T.J. & Purucker, M., 2002. On magnetic spectra of Earth and Mars, *J. geophys. Res.,* **107**, 5034, doi:10.1029/2001JE001534.

Wardinski, I., Holme, R., Asari, S. & Mandea, M., 2008. The 2003 geomagnetic jerk and its relation to core surface flows, *Earth planet. Sci. Lett.,* **267**, 468–481.

Whaler, K.A., 1980. Does the whole of Earth's core convect? *Nature,* **287**, 528–530.

Whaler, K. & Holme, R., 2007. Consistency between flow at the top of the core and the frozen-flux approximation, *Earth, Planets, Space,* **1**, 1219–1259.

Wicht, J., 2002. Inner-core conductivity in numerical dynamo simulations, *Phys. Earth planet. Inter.,* **132**, 281–302.

Wicht, J. & Tilgner, A., 2010. Theory and modeling of planetary dynamos, *Space Sci. Rev.,* **152**, doi:10.1007/s11214–010–9638–y.

APPENDIX: THE FLOW MAGNITUDE EQUATION IN SPECTRAL FORM

Assuming a source free region, the geomagnetic field due to internal sources can be represented in terms of the gradient of a magnetic potential $\boldsymbol{B} = -\nabla \Phi$ such that

$$\Phi = \sum_{l=1}^{\infty} \sum_{m=0}^{l} \Phi_l^m = \sum_{l=1}^{\infty} \sum_{m=0}^{l} a \left(\frac{a}{r}\right)^{l+1} \left[g_l^m(t) \cos m\phi \right.$$
$$\left. + h_l^m(t) \sin m\phi \right] P_l^m(\cos\theta), \qquad (A1)$$

where Φ_l^m are the spherical harmonic constituents of the scalar potential, r is the radius in kilometres, a is the spherical reference radius of the Earth's surface (6371.2 km), θ is co-latitude, ϕ is longitude, $P_l^m(\cos\theta)$ are associated Legendre polynomials of degree l and order m and $g_l^m(t)$ and $h_l^m(t)$ are the Gauss coefficients that define the field morphology at time t.

Following Mauersberger (1956) and Lowes (1966), the rms value of the vector field $\boldsymbol{B}$ on a spherical surface of radius c can be written as

$$\langle \boldsymbol{B} \rangle = \sqrt{\sum_{l=1}^{\infty} R_l(c)}, \tag{A2}$$

where

$$R_l(c) = (l+1)\left(\frac{a}{c}\right)^{2l+4} \sum_{m=0}^{l} \left[\left(g_l^m\right)^2 + \left(h_l^m\right)^2\right] \tag{A3}$$

is commonly referred to as the Mauersberger–Lowes spectrum. It indicates how the magnetic energy varies as a function of l at radius c. In the present context it is of interest to note that the rms value of B_r averaged over a sphere of radius c may also be written in terms of $R_l(c)$ as

$$\langle B_r \rangle = \sqrt{\sum_{l=1}^{\infty} \frac{(l+1)}{(2l+1)} R_l(c)}. \tag{A4}$$

A similar expression can also be written for the rms radial SV at $r = c$,

$$\langle \partial B_r / \partial t \rangle = \sqrt{\sum_{l=1}^{\infty} \frac{(l+1)}{(2l+1)} Q_l(c)}, \tag{A5}$$

where

$$Q_l(c) = (l+1)\left(\frac{a}{c}\right)^{2l+4} \sum_{m=0}^{l} \left[\left(\dot{g}_l^m\right)^2 + \left(\dot{h}_l^m\right)^2\right], \tag{A6}$$

with $\dot{g}_l^m(t)$ and $\dot{h}_l^m$ being the spherical harmonic coefficients of the SV.

It is also possible to directly obtain an expression for the rms values of $\nabla_H B_r$ on a spherical surface (where $\nabla_H = \nabla - \frac{\partial}{\partial r}\hat{\mathbf{r}}$) as follows. First note than one can write $\nabla_H B_r$ in terms of the spherical

harmonic constituents of the scalar potential Φ_l^m as,

$$\nabla_H B_r = \sum_{l=1}^{\infty} \sum_{m=0}^{l} \frac{(l+1)}{r} \nabla_H \Phi_l^m. \tag{A7}$$

Then, as demonstrated by Lowes (1966) (see his eqs 4 and 5), the mean square value of the non-radial part of the gradient of the scalar potential on a spherical surface of radius r is

$$\frac{1}{4\pi} \int_0^{2\pi} \int_0^{\pi} (\nabla_H \Phi_l^m) \cdot (\nabla_H \Phi_l^m) \sin\theta \, \mathrm{d}\theta \, \mathrm{d}\phi = \left(\frac{a}{r}\right)^{2l+4} \frac{l(l+1)}{(2l+1)} \times \left[\left(g_l^m\right)^2 + \left(h_l^m\right)^2\right]. \tag{A8}$$

The rms value of $\nabla_H B_r$ on the spherical surface $r = c$ is then

$$\langle \nabla_H B_r \rangle = \sqrt{\sum_{l=1}^{\infty} \frac{l(l+1)^3}{c^2(2l+1)} \left(\frac{a}{c}\right)^{2l+4} \left[\left(g_l^m\right)^2 + \left(h_l^m\right)^2\right]}$$

$$= \sqrt{\sum_{l=1}^{\infty} \frac{l(l+1)^2}{c^2(2l+1)} R_l(c)}. \tag{A9}$$

Taking c to be the radius of the Earth's core, and substituting (A5) and (A9) into (9) gives an expression for the rms value of $\boldsymbol{u}_H$ in terms of the MF spectrum $R_l(c)$ and the SV spectrum $Q_l(c)$ at the core surface,

$$\langle \boldsymbol{u}_H \rangle = \frac{\sqrt{\sum_{l=1}^{\infty} \frac{(l+1)}{(2l+1)} Q_l(c)}}{\sqrt{\sum_{l=1}^{\infty} \frac{l(l+1)^2}{c^2(2l+1)} R_l(c) \langle \cos\gamma \rangle}}. \tag{A10}$$

Note that this estimate depends only on the spectral properties of the observed magnetic field. Any phase information associated with the efficiency of induction is contained within the factor $\langle \cos\gamma \rangle$.